

Predicting low-temperature free energy landscapes with flat-histogram Monte Carlo methods

Nathan A. Mahynski, Marco A. Blanco, Jeffrey R. Errington, and Vincent K. Shen

Citation: *J. Chem. Phys.* **146**, 074101 (2017); doi: 10.1063/1.4975331

View online: <http://dx.doi.org/10.1063/1.4975331>

View Table of Contents: <http://aip.scitation.org/toc/jcp/146/7>

Published by the [American Institute of Physics](#)



**COMPLETELY
REDESIGNED!**

**PHYSICS
TODAY**

Physics Today Buyer's Guide
Search with a purpose.

Predicting low-temperature free energy landscapes with flat-histogram Monte Carlo methods

Nathan A. Mahynski,^{1,a)} Marco A. Blanco,¹ Jeffrey R. Errington,² and Vincent K. Shen¹

¹*Chemical Sciences Division, National Institute of Standards and Technology, Gaithersburg, Maryland 20899-8320, USA*

²*Department of Chemical and Biological Engineering, University at Buffalo, The State University of New York, Buffalo, New York 14260-4200, USA*

(Received 2 December 2016; accepted 20 January 2017; published online 15 February 2017)

We present a method for predicting the free energy landscape of fluids at low temperatures from flat-histogram grand canonical Monte Carlo simulations performed at higher ones. We illustrate our approach for both pure and multicomponent systems using two different sampling methods as a demonstration. This allows us to predict the thermodynamic behavior of systems which undergo both first order and continuous phase transitions upon cooling using simulations performed only at higher temperatures. After surveying a variety of different systems, we identify a range of temperature differences over which the extrapolation of high temperature simulations tends to quantitatively predict the thermodynamic properties of fluids at lower ones. Beyond this range, extrapolation still provides a reasonably well-informed estimate of the free energy landscape; this prediction then requires less computational effort to refine with an additional simulation at the desired temperature than reconstruction of the surface without any initial estimate. In either case, this method significantly increases the computational efficiency of these flat-histogram methods when investigating thermodynamic properties of fluids over a wide range of temperatures. For example, we demonstrate how a binary fluid phase diagram may be quantitatively predicted for many temperatures using only information obtained from a single supercritical state. [<http://dx.doi.org/10.1063/1.4975331>]

I. INTRODUCTION

When cooled from a high temperature state, many physical systems undergo phase transitions^{1,2} that may be classified as either first-order or continuous transitions.^{2,3} First-order phase transitions are characterized by a discontinuous change in the first derivative of the free energy across the transition. For instance, when a fluid condenses or crystallizes, its density changes discontinuously during the phase change. Continuous transitions do not display a discontinuity and are instead characterized by a divergent order parameter susceptibility and correlations length, with a power-law decay of these correlations near critical points.³ Some examples of this include the spontaneous magnetization of ferromagnetic materials, superconductivity, and the self-assembly of amphiphiles.

Understanding first-order fluid phase transitions is of key importance in numerous fields. These transitions form the foundation of many industrial chemical separation processes such as distillation and adsorption.^{1,4-7} They also play a key role in chemical and pharmaceutical manufacturing⁷⁻⁹ and have even been shown to control the organization of materials inside cells.^{10,11} Similarly, second and higher order phase transitions play a major role in designing soft reconfigurable materials,¹²⁻¹⁹ engineering pharmaceutical delivery systems,²⁰ controlling the micellization of surfactants,²¹⁻²³ and understanding protein folding and self-association.²⁴

Yet experimental investigations of phase transitions often struggle to provide insight into the microscopic details of these phenomena, and many idealized theoretical models inadequately represent the thermodynamics of realistic systems; consequently, computer simulations have become a valuable tool for investigating these transitions.

Monte Carlo (MC) simulations are particularly well-suited to studying the thermodynamic properties of fluid phases, and a plethora of different techniques have been developed over the past half century.^{2,25-27} In particular, Gibbs ensemble simulations are highly effective at establishing coexistence properties of subcritical systems that undergo first order fluid-fluid phase transitions, except near a critical point.^{26,28} Grand canonical Monte Carlo (GCMC), in concert with finite-size scaling, is more efficient near criticality.^{26,29,30} Histogram reweighting techniques often greatly increase the computational efficiency of GCMC simulations as they allow one to predict the behavior of a system at other externally imposed conditions, e.g., temperature or chemical potential.²⁶ However, this increase in efficiency is limited by how far one can accurately reweight data obtained at some reference condition, which is determined by the breadth of phase space which can be effectively sampled at the reference state. Reweighting large differences in temperature, for instance, is therefore often very difficult as the most important regions of phase space can shift significantly.³¹

Flat-histogram techniques, such as Wang-Landau (WL)³² or transition matrix Monte Carlo (TMMC),³³⁻³⁵ use biased

^{a)}Electronic mail: nathan.mahynski@nist.gov

sampling to explore an entire range of predefined phase space according to one or more order parameters chosen. Consequently, they provide complete information about this phase space by constructing the (logarithm of the) relative probability, $\ln \Pi(\vec{\Psi})$, of all macrostates in that space defined by some set of order parameters, $\vec{\Psi}$. However, these order parameters must be chosen carefully so that they range over all physically accessible and meaningful states of the particular system in question, and should capture the phase transition being studied. For fluids, energy is a particularly troublesome space to cover as its bounds are not often known *a priori* as a function of other thermodynamic variables, and is generally continuous unlike, e.g., particle number which is discrete. Therefore, its thermodynamic conjugate, $\beta \equiv 1/k_B T$ (k_B is the Boltzmann constant and T is temperature), can be a cumbersome variable to employ in reweighting schemes, and obtaining thermodynamic properties about systems at very low temperatures from simulations at higher ones can be difficult.

Direct simulations of fluid systems at lower temperatures tend to be much more difficult than those at higher temperatures because of large activation energy barriers between different states, i.e., long tunneling times. Even flat-histogram approaches which are designed to have inherently low tunneling times, such as Wang-Landau or metadynamics,^{2,27,32,36,37} struggle to converge for many systems at very low temperatures. However, if a good initial guess of the $\ln \Pi(\vec{\Psi})$ surface can be provided *a priori*, convergence can be greatly accelerated. Other approaches, such as expanded-ensemble techniques and intelligently biased MC moves including Rosenbluth sampling for polymers,²⁷ aggregation volume bias,^{38,39} and cluster moves^{40,41} often help ameliorate the problem by increasing the computational efficiency of MC simulations, but are not a panacea.

In this work, we present a method by which the macrostate distribution of an open system may be extrapolated from one temperature to another, which enables us to circumvent these difficulties and increase the computational efficiency of flat-histogram methods commonly used to study fluid phase behavior. We derive expressions for the thermodynamic partial derivatives of the macrostate distribution with respect to temperature in two different ensembles, which allows us to construct a Taylor series expansion of the $\ln \Pi(\vec{\Psi})$ surface at each discrete macrostate defined by the ensemble's order parameter. The order parameters we employ are different for each ensemble, but are based on particle numbers, which are discrete, and therefore have well-defined bounds. Here, we focus on relatively simple models for bulk and confined fluids, as well as "patchy" particles, which can be used as coarse-grained models of proteins. These systems exhibit first order phase transitions, capillary condensation, and self-assembly in the case of patchy particles. We demonstrate how high-temperature simulations can be used to predict the free energy landscape and resulting thermodynamic properties of these systems at much lower temperatures where phase transitions occur. In many instances, these predictions are accurate enough to directly calculate fluid properties; in other instances, these predictions serve as initial guesses of $\ln \Pi(\vec{\Psi})$ which can be subsequently

refined with additional simulations at reduced computational expense.

The remainder of this paper is organized as follows. In Sec. II we discuss two different multicomponent sampling approaches and review the particular flat-histogram Monte Carlo technique we employ here. We then present the results of the derivations which permit the extrapolation of the macrostate distribution for a general k -component system from one temperature to another. The complete derivations are relegated to Appendices A and B in the interest of brevity. In Sec. III we demonstrate our approach by applying it to both pure component bulk fluids and mixtures, which undergo first order phase separations upon cooling, using both ensembles discussed in Sec. II to demonstrate their equivalence. Subsequently, we demonstrate how these equations may be employed to predict capillary condensation and prewetting phase behavior. We then apply our approach to the study of self-assembling patchy systems to demonstrate its capacity to predict higher order transitions. Finally, we conclude in Sec. IV and offer some perspective and outlook for future work.

II. METHODS

A. Thermodynamic ensembles

We consider a multicomponent fluid system composed of particles at fixed temperature, $\beta = 1/k_B T$, volume, V , and chemical potentials, $\vec{\mu} = (\mu_1, \mu_2, \dots, \mu_k)$, for each species in a k -component mixture. The partition function, $\Xi(\beta, V, \vec{\mu})$, for such a system may be expressed as

$$\Xi(\beta, V, \vec{\mu}) = \sum_{N_1} \exp(\beta \mu_1 N_1) \dots \sum_{N_k} \exp(\beta \mu_k N_k) Q(\beta, V, \vec{N}), \quad (1)$$

where $Q(\beta, V, \vec{N})$ is the canonical partition function for a system at fixed temperature, volume, and particle number, $\vec{N} = (N_1, N_2, \dots, N_k)$. The natural logarithm of the probability of observing a macrostate, defined by the number of each species present, is given by

$$\ln \Pi(\vec{N}; \beta, V, \vec{\mu}) = \beta \sum_{i=1}^k \mu_i N_i + \ln Q - \ln \Xi. \quad (2)$$

Given a known macrostate distribution, $\ln \Pi(\vec{N}; \beta, V, \vec{\mu}^0)$, at one set of imposed chemical potentials, $\vec{\mu}^0$, standard histogram reweighting techniques can be used to recalculate it at any other given set, $\vec{\mu}$,

$$\ln \Pi(\vec{N}; \vec{\mu}) = \ln \Pi(\vec{N}; \vec{\mu}^0) + \beta \sum_{i=1}^k (\mu_i - \mu_i^0) N_i + C, \quad (3)$$

where $C = -\ln \Xi/\Xi^0$ which is a constant that may be neglected. This macrostate distribution is then segmented at local minima to divide different phases.⁴² Only the parts of the surface belonging to a certain phase contribute to the properties of that phase. Ensemble-averaged extensive properties, $\langle X \rangle$, may be obtained as weighted averages of that property as a function of the macrostate, \vec{X} ,

$$\langle X^a \rangle = \frac{\sum_{N_1 \in a} \dots \sum_{N_k \in a} \Pi(\vec{N}) \tilde{X}(\vec{N})}{\sum_{N_1 \in a} \dots \sum_{N_k \in a} \Pi(\vec{N})}, \quad (4)$$

where a denotes the phase in question. Intensive quantities are simply ratios of extensive ones, e.g., for a binary mixture $x_1 = \langle N_1 \rangle / (\langle N_1 \rangle + \langle N_2 \rangle)$. Coexistence between two phases, a and b , is defined for a fixed set of chemical potentials, $\vec{\mu}$, when

$$\ln \sum_{N_1 \in a} \dots \sum_{N_k \in a} \Pi(\vec{N}) = \ln \sum_{N_1 \in b} \dots \sum_{N_k \in b} \Pi(\vec{N}). \quad (5)$$

This is equivalent to the condition of mechanical equilibrium, requiring that the pressures of the two phases be equal, since

$$P^a = \frac{\ln \Xi}{\beta V} = \frac{\ln \sum_{N_1 \in a} \dots \sum_{N_k \in a} \Pi(\vec{N}) / \Pi(\vec{0})}{\beta V}, \quad (6)$$

where $\Pi(\vec{0})$ denotes the value of the macrostate when there are no particles in the system, i.e., $\vec{N} = \vec{0}$, at a given β , V , $\vec{\mu}$.⁴³

However, it is sometimes more convenient to work in a slightly modified ensemble where the total particle number, $N_{\text{tot}} = \sum_i N_i$, can be taken as the order parameter. This reduces the number of order parameters needed for multicomponent systems and has straightforward bounds; whereas, for a highly size-asymmetric multicomponent system, simultaneously enumerating all valid possible combinations of particle numbers is difficult or impossible to know *a priori*. It is possible to express Eq. (1) as follows:

$$\Xi(\beta, V, \vec{\mu}) = \sum_{N_{\text{tot}}} \exp(\beta \mu_1 N_{\text{tot}}) \sum_{N_2} \exp(\beta \Delta \mu_2 N_2) \dots \times \sum_{N_k} \exp(\beta \Delta \mu_k N_k) Q(\beta, V, \vec{N}) \quad (7)$$

$$= \sum_{N_{\text{tot}}} \exp(\beta \mu_1 N_{\text{tot}}) \Upsilon(\beta, V, N_{\text{tot}}, \Delta \vec{\mu}), \quad (8)$$

where $\Upsilon(\beta, V, N_{\text{tot}}, \Delta \vec{\mu})$ is the isochoric semigrand partition function,^{44,45} and $\Delta \mu_i \equiv \mu_i - \mu_1$. As a result, we may express the probability of a given macrostate as

$$\ln \Pi(N_{\text{tot}}; \beta, V, \mu_1, \Delta \vec{\mu}) = \beta \mu_1 N_{\text{tot}} + \ln \Upsilon - \ln \Xi. \quad (9)$$

This is equivalent to Eq. (2), but it can be significantly simpler to implement in simulations as we now have a scalar order parameter.^{34,35} At a fixed $\Delta \vec{\mu}$, this distribution may be reweighted to new μ_1 values according to

$$\ln \Pi(N_{\text{tot}}; \mu_1) = \ln \Pi(N_{\text{tot}}; \mu_1^0) + \beta(\mu_1 - \mu_1^0)N_{\text{tot}}, \quad (10)$$

where the trailing constant related to Ξ has been neglected. Here, we have implemented both methods to demonstrate their equivalence, and to illustrate how temperature extrapolation of $\ln \Pi(\vec{\Psi})$ works in both instances.

B. Simulations

Although a variety of flat-histogram methods exist, here we employ a technique known as Wang-Landau Transition Matrix Monte Carlo (WL-TMMC) to construct $\ln \Pi(\vec{\Psi})$. This technique is already described in detail elsewhere,^{33,34,46} but we summarize the approach here. Wang-Landau (WL) simulations are used to build an initial guess of the macrostate distribution since this technique has a relatively low tunneling time during the early stages of the simulation. However,

these simulations tend to converge slowly. The opposite tends to be true of Transition Matrix Monte Carlo (TMMC); therefore, these techniques can be combined by using an initial WL stage to build up an approximate $\ln \Pi(\vec{\Psi})$ surface, which is subsequently refined with TMMC.

The probability of observing a given microstate, s , in the grand canonical ensemble with k -components is

$$\pi(s) = \frac{\exp(-\beta U(s))}{\Xi} \prod_{i=1}^k \frac{V^{N_i(s)} \exp(\beta \mu_i N_i(s))}{N_i(s)!}, \quad (11)$$

where $U(s)$ is the potential energy of the microstate. The unbiased Metropolis acceptance criteria of moving from one microstate, “ x ”, to another, “ y ”, is then

$$p_u = \min \left[1, \frac{\pi(y)}{\pi(x)} \right]. \quad (12)$$

In flat-histogram sampling, a proposed move is accepted with a probability that is biased by some function, $\eta(\vec{\Psi})$, which depends on the order parameter we have selected, $\vec{\Psi}$. When we wish to construct $\ln \Pi(\vec{N})$, $\vec{\Psi} = \vec{N}$; whereas if we wish to construct $\ln \Pi(N_{\text{tot}})$, $\vec{\Psi} = N_{\text{tot}} = \sum_{i=1}^k N_i$. Flat-histogram methods seek to construct the $\ln \Pi(\vec{\Psi})$ surface by iteratively converging this biasing function so that it is the inverse of the macrostate distribution. Simulations proceed by accepting moves weighted by this bias so that the biased probability of observing any macrostate is constant once $\eta(\vec{\Psi})$ has converged,

$$p_{\text{bias}} = \min \left[1, \frac{\exp(\eta[\vec{\Psi}(y)]) \pi(y)}{\exp(\eta[\vec{\Psi}(x)]) \pi(x)} \right]. \quad (13)$$

Thus, once converged the biasing function provides the macrostate distribution, according to

$$\eta(\vec{\Psi}) = -\ln \Pi(\vec{\Psi}). \quad (14)$$

Initially, $\eta(\vec{\Psi})$ is set to zero for all values of $\vec{\Psi}$ and constructed using WL. As the simulation proceeds, different Monte Carlo moves are made; after each move, the estimated macrostate distribution (inverse of the bias) is incremented by an update factor, f ,

$$\ln \Pi(\vec{\Psi}) = \ln \Pi(\vec{\Psi}) + \ln f. \quad (15)$$

Initially $\ln f = 1$, but is reduced as the simulation converges. Convergence is estimated by recording a visited-states histogram, $H(\vec{\Psi})$, which monitors how often each macrostate has been visited. When the minimum of $H(\vec{\Psi})$ is within 80% of the mean value, $\ln f$ is reduced by a factor of 2, and $H(\vec{\Psi})$ is reset to zero for each macrostate. This is repeated until $\ln f < 10^{-8}$ to build up an initial guess of $\ln \Pi(\vec{\Psi})$, before refinement with TMMC.

TMMC constructs its estimate of the macrostate distribution differently. In this method, a collection matrix C is recorded, which accumulates statistics about the unbiased probability of transitioning between macrostates. The simulation proceeds according to the biased acceptance criteria in

Eq. (13), with C being updated after every attempted move, regardless the outcome, via the following rules:

$$C[\vec{\Psi}(x) \rightarrow \vec{\Psi}(y)] = C[\vec{\Psi}(x) \rightarrow \vec{\Psi}(y)] + p_u, \quad (16)$$

$$C[\vec{\Psi}(x) \rightarrow \vec{\Psi}(x)] = C[\vec{\Psi}(x) \rightarrow \vec{\Psi}(x)] + 1 - p_u. \quad (17)$$

From the collection matrix, one can reconstruct the transition probability, $P[x \rightarrow y]$, of going from macrostate “ x ” to “ y ” by normalizing the accumulated unbiased probabilities of this transition over all possible transitions which originated from macrostate “ x ,”

$$P[x \rightarrow y] = \frac{C[\vec{\Psi}(x) \rightarrow \vec{\Psi}(y)]}{\sum_m C[\vec{\Psi}(x) \rightarrow \vec{\Psi}(m)]}. \quad (18)$$

The estimated macrostate distribution (inverse of the bias) is then known from the detailed balance condition,

$$\ln \Pi[\vec{\Psi}(y)] = \ln \Pi[\vec{\Psi}(x)] + \frac{P[\vec{\Psi}(x) \rightarrow \vec{\Psi}(y)]}{P[\vec{\Psi}(y) \rightarrow \vec{\Psi}(x)]}. \quad (19)$$

The TMMC portion of the simulation is run long enough to allow P to converge, after which $\ln \Pi(\vec{\Psi})$ is obtained from Eq. (14). It is clear, however, that when $\vec{\Psi}$ is not a scalar quantity and there exist multiple “routes” from macrostate “ x ” to “ y ,” it is not simple to reconstruct $\ln \Pi(\vec{\Psi})$ and optimization methods to minimize the error associated with the violation of detailed balance must be employed.³⁴ Directed sampling along fixed routes or grids can help assist in this endeavor, and has been detailed in Ref. 34. We adopt this approach here to prove its equivalence to that of Ref. 35, in which $\vec{\Psi} = N_{\text{tot}}$. Regardless of the $\vec{\Psi}$ chosen, we also record extensive thermodynamic properties as a function of the order parameter during the simulations, as well as the products of different properties. As we will show next, these will be necessary for the extrapolation of $\ln \Pi(\vec{\Psi})$ and extensive properties, $\tilde{X}(\vec{\Psi})$, to different temperatures.

C. Temperature extrapolation

In order to predict the macrostate distribution, $\ln \Pi(\vec{\Psi})$, at temperatures different from the simulation temperature, we expand it in a Taylor series up to some order, ξ_t ,

$$\begin{aligned} \ln \Pi(\vec{\Psi}; \beta) &= \ln \Pi(\vec{\Psi}; \beta^0) \\ &+ \left. \frac{\partial \ln \Pi(\vec{\Psi})}{\partial \beta} \right|_{\beta^0} \Delta\beta + \frac{1}{2!} \left. \frac{\partial^2 \ln \Pi(\vec{\Psi})}{\partial \beta^2} \right|_{\beta^0} \Delta\beta^2 \\ &+ \dots, \end{aligned} \quad (20)$$

where $\Delta\beta = \beta - \beta^0$ and β^0 corresponds to the (inverse) simulation temperature. A full derivation of the partial derivatives for each term required is presented in Appendices A and B for the interested reader. Here we present the results directly for the sake of brevity. To evaluate these partial derivatives, extensive properties and permutations of their products raised to integer powers, such as N_1 , $U^2 N_2$, and $N_1 N_2 U$, must be collected in a histogram at each value of the order parameter, $\vec{\Psi}$. For a pure component system, we require

$$W(\vec{\Psi}; \xi) = N_1^{\xi_1}(\vec{\Psi}) U^{\xi_u}(\vec{\Psi}), \quad (21)$$

where $\vec{\xi} = (\xi_1, \xi_u)$. Here, ξ_1 and ξ_u are non-negative integer powers. We point out that throughout this manuscript we take U to refer only to the potential energy of the system. This is done for mathematical convenience, as it simplifies the expressions for the derivatives and does not incur any loss of generality (cf. Appendices A and B). Kinetic energy effects may be incorporated into this approach; however, this incurs additional complexity which is beyond the scope of this paper and is the subject of forthcoming work. Extrapolation of $\ln \Pi(\vec{\Psi})$ requires all terms that satisfy $\xi_1 + \xi_u \leq \xi_t$. However, to extrapolate extensive property histograms to the same order, ξ_t , we require all $\xi_1 + \xi_u \leq \xi_t + 1$. Therefore, we measure all $\xi_i \in [0, \xi_t + 1]$. In spite of this, the order with which the macrostate distribution and extensive property histograms are extrapolated need not be the same, and we have generally found that extensive property extrapolation can be done at a lower order than $\ln \Pi(\vec{\Psi})$ while remaining accurate. For a k -component system, we must collect all

$$W(\vec{\Psi}; \vec{\xi}) = N_1^{\xi_1}(\vec{\Psi}) N_2^{\xi_2}(\vec{\Psi}) \dots N_k^{\xi_k}(\vec{\Psi}) U^{\xi_u}(\vec{\Psi}), \quad (22)$$

where $\vec{\xi} = (\xi_1, \dots, \xi_k, \xi_u)$. Again, we record all $\xi_i \in [0, \xi_t + 1]$ since to reach a desired order of extrapolation one requires $\sum \xi_i \leq \xi_t$, and one order higher for the corresponding extensive property extrapolation. In the case where the order parameter is given by the set of all particle numbers, $\vec{\Psi} = \vec{N}$, we have

$$\frac{\partial \ln \Pi(\vec{N})}{\partial \beta} = \sum_{i=1}^k \mu_i (N_i - \langle N_i \rangle) - (\tilde{U} - \langle U \rangle). \quad (23)$$

The second order term may be expressed as

$$\frac{\partial^2 \ln \Pi(\vec{N})}{\partial \beta^2} = - \sum_{i=1}^k \mu_i \frac{\partial \langle N_i \rangle}{\partial \beta} - \frac{\partial \tilde{U}}{\partial \beta} + \frac{\partial \langle U \rangle}{\partial \beta}, \quad (24)$$

in which

$$\frac{\partial \langle W \rangle}{\partial \beta} = \sum_{i=1}^k \mu_i \hat{f}(\langle W \rangle, \langle N_i \rangle) - \hat{f}(\langle W \rangle, \langle U \rangle), \quad (25)$$

where $\langle W \rangle$ and \tilde{W} denote average extensive quantities in different ensembles. The former is the grand canonical average of some property which may be raised to some integer exponent, e.g., $\langle W \rangle = \langle U^3 \rangle$ or $\langle W \rangle = \langle N_1^2 U \rangle$, whereas the latter refers to the canonical ensemble average of W . Average quantities in the grand canonical ensemble are calculated from Eq. (4), whereas average quantities in the canonical ensemble are simply the values obtained from the corresponding extensive property histograms recorded at a given order parameter value. We use the notation $\hat{f}(\langle X \rangle, \langle Y \rangle)$ to denote the fluctuation of extensive properties $\langle X \rangle$ and $\langle Y \rangle$ in the grand canonical ensemble, such that $\hat{f}(\langle X \rangle, \langle Y \rangle) = \langle XY \rangle - \langle X \rangle \langle Y \rangle$. It follows directly that

$$\frac{\partial \hat{f}(\langle X \rangle, \langle Y \rangle)}{\partial \beta} = \frac{\partial \langle XY \rangle}{\partial \beta} - \langle X \rangle \frac{\partial \langle Y \rangle}{\partial \beta} - \langle Y \rangle \frac{\partial \langle X \rangle}{\partial \beta}. \quad (26)$$

Higher order derivatives of the canonical average potential energy at each \vec{N} may be obtained by utilizing the fact that

$$\frac{\partial \tilde{U}^{\xi_u}}{\partial \beta} = -\tilde{f}(\tilde{U}^{\xi_u}, \tilde{U}), \quad (27)$$

where $\tilde{f}(\tilde{X}, \tilde{Y})$ is used to denote the fluctuation of extensive properties \tilde{X} and \tilde{Y} in the canonical ensemble, such that $\tilde{f}(\tilde{X}, \tilde{Y}) = \tilde{X}\tilde{Y} - \langle \tilde{X}\tilde{Y} \rangle$. Thus, akin to Eq. (26), derivatives of fluctuations in this ensemble are given by

$$\frac{\partial \tilde{f}(\tilde{U}^{\xi_u}, \tilde{U})}{\partial \beta} = -\tilde{f}(\tilde{U}^{\xi_u+1}, \tilde{U}) + \tilde{U}\tilde{f}(\tilde{U}^{\xi_u}, \tilde{U}) + \tilde{U}^{\xi_u}\tilde{f}(\tilde{U}, \tilde{U}). \quad (28)$$

By recursive application of Eqs. (25)–(28), all higher order terms may be obtained, given that the appropriate quantities have been sampled during the simulation. Since the set of particle numbers is the order parameter in this case, the only extensive quantity that must be extrapolated as temperature changes is \tilde{U} ; however, this is only required if one wishes to calculate $\langle U \rangle$ at the new temperature, and it is not necessary for the calculation of $\ln \Pi(\tilde{\Psi})$. A simple Taylor series may again be used, using Eq. (27), to evaluate the necessary derivatives.

In the case where the order parameter is chosen to be the scalar N_{tot} instead, the first two derivatives of the macrostate distribution become

$$\frac{\partial \ln \Pi(N_{\text{tot}})}{\partial \beta} = \mu_1 (N_{\text{tot}} - \langle N_{\text{tot}} \rangle) + \sum_{i=1}^k \Delta \mu_i (\tilde{N}_i - \langle N_i \rangle) - (\tilde{U} - \langle U \rangle), \quad (29)$$

$$\frac{\partial^2 \ln \Pi(N_{\text{tot}})}{\partial \beta^2} = -\mu_1 \frac{\partial \langle N_{\text{tot}} \rangle}{\partial \beta} + \sum_{i=1}^k \Delta \mu_i \left(\frac{\partial \tilde{N}_i}{\partial \beta} - \frac{\partial \langle N_i \rangle}{\partial \beta} \right) - \left(\frac{\partial \tilde{U}}{\partial \beta} - \frac{\partial \langle U \rangle}{\partial \beta} \right). \quad (30)$$

By definition, $\Delta \mu_1 = 0$, and hence the first term in the above sums may be neglected; we include it only for notational convenience. Similarly, the requisite derivatives to evaluate these terms are given by

$$\frac{\partial \langle Z \rangle}{\partial \beta} = \mu_1 \hat{f}(\langle Z \rangle, \langle N_{\text{tot}} \rangle) + \sum_{i=1}^k \Delta \mu_i \hat{f}(\langle Z \rangle, \langle N_i \rangle) - \hat{f}(\langle Z \rangle, \langle U \rangle) \quad (31)$$

and

$$\frac{\partial \tilde{Z}}{\partial \beta} = \sum_{i=1}^k \Delta \mu_i \tilde{f}(\tilde{Z}, \tilde{N}_i) - \tilde{f}(\tilde{Z}, \tilde{U}). \quad (32)$$

In this ensemble, \tilde{Z} refers to an average extensive quantity (or product thereof) in the isochoric semigrand ensemble. Z may be contained in the W matrix, or it may be a product of a term in the matrix and the order parameter, N_{tot} , raised to an integer power, ξ_n , which is necessary to evaluate, e.g., $\partial \langle N_{\text{tot}} \rangle / \partial \beta$,

$$Z(\tilde{\Psi}; \vec{\xi}) = N_1^{\xi_1}(\tilde{\Psi}) N_2^{\xi_2}(\tilde{\Psi}) \dots N_k^{\xi_k}(\tilde{\Psi}) N_{\text{tot}}^{\xi_n}(\tilde{\Psi}) U^{\xi_u}(\tilde{\Psi}), \quad (33)$$

where now $\vec{\xi} = (\xi_1, \dots, \xi_k, \xi_n, \xi_u)$. Note that for a pure component system, Z and W are essentially identical since $N_{\text{tot}} = N_1$. The chain rule is equally valid for these expressions and Eq. (26) may be used recursively again, in conjunction with Eqs. (31) and (32), to determine higher order derivatives of $\ln \Pi(\tilde{\Psi})$ and the extensive properties.

It should now be clear how the exponents on extensive properties in the Z and W matrices arise. Summarily, first derivatives of the macrostate distribution, regardless of the order parameter, involve average extensive properties, e.g., consider Eq. (29). Second derivatives involve fluctuations of those properties (cf. Eqs. (30)–(32)), while higher derivatives involve fluctuations of those fluctuations and so on. By inspection of Eqs. (26) and (28) it is clear that the derivative of a fluctuation of two extensive properties, X and Y , involves taking the product of these properties. Thus, obtaining higher order derivatives of the macrostate distribution requires averages of the repeated products of such properties, leading to the necessity of higher powers in the Z and W matrices.

We point out that the macrostate distribution does not need to be segmented into phases before extrapolation even if multiple phases are present at the temperature where the initial simulation was performed; one simply applies Eq. (20) to the entire $\ln \Pi(\tilde{\Psi})$ distribution, after which segmentation into phases is done, if they exist. We also note that extrapolation to finite order inherently introduces some error. This problem can be mitigated if the macrostate distribution is first reweighted using Eq. (3) or (10) before extrapolating $\ln \Pi(\tilde{\Psi})$ to a different temperature. Simplified expressions for up to second order terms ($\xi_t = 2$) in Eq. (20) for both ensembles are given in [Appendices A and B](#).

III. RESULTS

A. Pure component fluid phase behavior

Consider a square-well fluid⁴⁷ where the interparticle potential between a particle of species i and j is given by

$$U_{i,j}(r) = \begin{cases} \infty, & r < \sigma_{i,j}, \\ -\epsilon_{i,j}, & \sigma_{i,j} \leq r < \sigma_{i,j}\lambda_{i,j}, \\ 0, & r \geq \sigma_{i,j}\lambda_{i,j}, \end{cases} \quad (34)$$

As an initial comparison, we explore the accuracy of our extrapolation method for a single component fluid with $\epsilon_{1,1} = 1$, $\sigma_{1,1} = 1$, and $\lambda_{1,1} = 1.5$. This fluid has a critical point at $k_B T_{c,1} / \epsilon_{1,1} \approx 1.22$.^{47,48} Note that for pure component systems, $N_{\text{tot}} = N$ and the ensembles described above produce identical expansions of $\ln \Pi(N)$ as a function of β . As a proof of concept, we performed a number of WL-TMMC simulations at different temperatures such that $T^* = k_B T / \epsilon_{1,1} = 1.05, 1.10, 1.15, 1.20, 1.30, 1.35$; here we limit our discussion to representative results. Fig. 1(a) depicts a comparison between direct simulations (points) obtained at $T^* = 1.05$ and those extrapolated from simulations performed at $T^* = 1.35$ (lines). This is the largest difference between the temperatures we have simulated. For a desired chemical potential, the distribution at $T^* = 1.35$ is first reweighted to the desired μ_1 before extrapolation is performed. Performing this sequence in the reverse order entails reweighting extrapolated data, which tends to amplify errors. To the naked eye, both first order and second order expansions of the $\ln \Pi(N)$ surface at all chemical potentials seem to agree well with those obtained via direct simulation at lower T^* . Closer inspection reveals a systematic deviation in the tunneling region of $\ln \Pi(N)$ between a

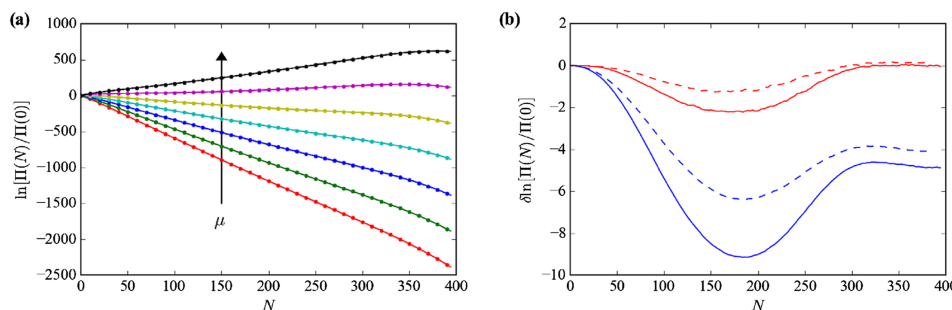


FIG. 1. (a) Comparison between direct simulations (points) of the pure component square-well fluid at $T^* = 1.05$ and extrapolation from $T^* = 1.35$ (lines) over the range $-10 \leq \mu/\epsilon_{1,1} \leq -2$. (b) Difference between the extrapolated results and those obtained via direct simulation, such that $\delta \ln[\Pi(N)/\Pi(0)] \equiv \ln[\Pi(N)/\Pi(0)]_{\text{ext}} - \ln[\Pi(N)/\Pi(0)]_{\text{sim}}$. Dashed lines correspond to $\epsilon_{1,1} = 0.93$ (increased T^*) instead of $\epsilon_{1,1} = 1$. Blue and red curves correspond to the use of first and second order corrections, respectively.

high and low density state, which at low temperatures represent the liquid and vapor states, respectively. Including second order corrections decreases the maximum error in this region by nearly an order of magnitude over the case when only a first order expansion is used. Fig. 1(b) depicts a comparison in the error between direct simulation and extrapolation from the supercritical state for $\epsilon_{1,1} = 1$ and $\epsilon_{1,1} = 0.93$ when $k_B T = 1.35$. In this case, the maximum error is always less than when $\epsilon_{1,1}$ is larger, but is also reduced by a similar magnitude as higher order corrections are introduced. Note that by reweighting $\ln \Pi(N)$ before extrapolating it, the error is essentially independent of the chemical potential we choose. This is because reweighting produces an “exact” distribution at the new chemical potential since there are no approximations involved. The error shown in Fig. 1(b) comes purely from the extrapolation in temperature.

Representative isotherms obtained by extrapolating supercritical simulation data from $T^* = 1.35$ as low as $T^* = 1.05$ are shown in Fig. 2. There is a quantitative agreement between the isotherms at all temperatures we have considered here; these isotherms clearly show a bulk phase separation below a critical temperature of $T_{c,1}^* \approx 1.22$. The binodal for these subcritical temperatures can also be easily located using extrapolation of supercritical data. Following this, the enthalpy of vaporization can be obtained from the Clausius-Clapeyron expression by plotting $\ln P^{\text{sat}}$ vs. $1/k_B T$ (cf. inset of Fig. 3(b)).

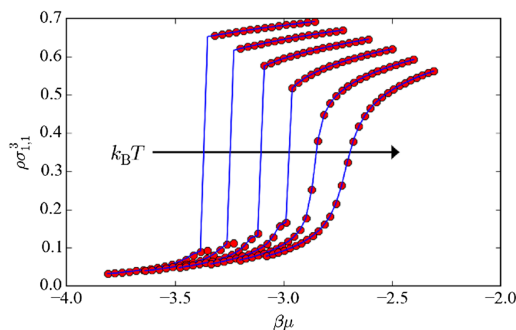


FIG. 2. Comparison between isotherms for the pure component square-well fluid obtained by direct simulations (blue lines) at subcritical temperatures ($1.05 \leq T^* \leq 1.30$ in increments of 0.05) and those produced as a result of extrapolation from a single simulation at $T^* = 1.35$ (red points). Standard errors are less than symbol size from five total replicates.

Fig. 3 illustrates the results when data collected from a simulation at $T^* = 1.35$ are used to predict saturation properties at subcritical temperatures. These results correspond to Fig. 2. In Fig. 3(a) the macrostate distribution is shown for various temperatures to compare direct simulation (solid lines) to predictions from extrapolated data (dashed lines). Consistent with Fig. 1, the extrapolation tends to overestimate the depth of the minimum separating the two local maxima; however, the error is significantly reduced as the maxima are approached. This implies that the phase behavior, or any calculation concerned with the most likely macrostates, is expected to be quite accurate. However, if we are interested in calculating properties which depend on the tunneling region (transition state), the error is expected to be higher. For example, following Binder’s formalism,⁴⁹ the surface tension between two fluid phases may be calculated as the mean of the difference between the local maxima in $\ln \Pi(\vec{\Psi})$ representing each phase, and the minima between them.^{49,50} Such a calculation would be expected to become progressively less accurate as we extrapolate a macrostate distribution further from the measurement temperature because $\ln \Pi(\vec{\Psi})$ is poorly estimated in the region between the two phases. However, as expected, if one calculates the saturation properties (cf. Fig. 3(b)) there is essentially no difference between results obtained from direct simulation and those from extrapolated data. Similarly, we expect that alternative approaches such as the interface-potential-based approach,⁵¹ which rely only on properties of phases rather than the transition region between them, will benefit from the use of this extrapolation method. This is particularly relevant as such approaches often require expanded ensemble simulations or other special sampling techniques to investigate low temperatures.^{51,52}

Generally, the error in the extrapolated data grows as $\Delta\beta$ increases. However, as the error in the macrostate distribution primarily arises in highly correlated regions, it is anticipated that this error is related to the accuracy on the measurements of those correlations. For example, very near the critical point the fluctuations will be most pronounced in the simulation; we found that performing simulations just above or below this point tends to produce the most accurate extrapolations. Consider Fig. 3(c) in which we have depicted the average error (cf. both the liquid and vapor branches) between the saturation densities obtained by direct simulation and extrapolation from

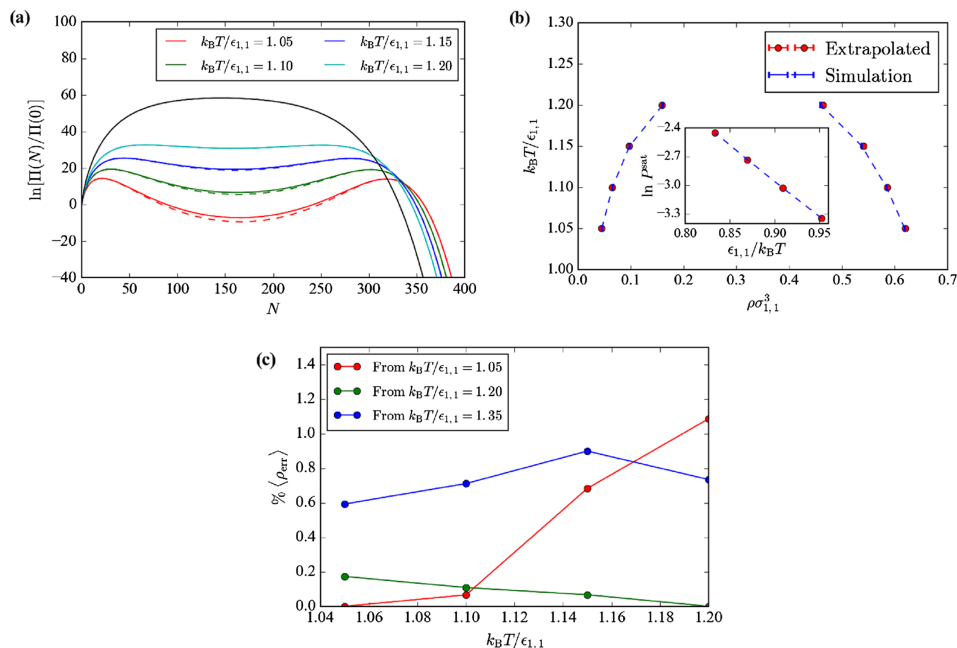


FIG. 3. (a) Macrostate distributions for the pure component square-well fluid obtained from direct simulation (solid lines) and from extrapolating data (dashed lines) obtained at $T^* = 1.35$ (black solid line). (b) Liquid-vapor coexistence densities from direct simulation and extrapolation from $T^* = 1.35$. The standard error from five total replicates is reported at each point; however, it is generally much less than symbol size. (c) Absolute value of the difference between the replicate-averaged saturation densities for direct simulation and extrapolation estimates when the extrapolation is performed starting from different reference temperatures.

different reference temperatures. In each case, four additional replicates were performed to obtain statistical averages. The blue curve represents the case we have focused on until this point, that is, using the supercritical data as a reference from which to extrapolate. Over the range of temperatures we have investigated, the average error does not change very significantly and remains on the order of 1% or less; this invariance is again, due to the fact that the error in the macrostate distribution primarily accumulates in the tunneling region between the coexisting phases rather than around the macrostates which principally define the phases. However, if we instead use data collected at $T^* = 1.05$ as a reference (red curve), we indeed observe that the error grows as T^* increases, especially as the critical point is approached. Most notably, if we use data collected just below the critical point at $T^* = 1.20$ the average error in the saturation densities is almost an order of magnitude less over the temperature range investigated. We attribute this to the fact that near the critical point, the simulation samples large fluctuations. Hence, we suggest that if a critical point, or other temperature at which large fluctuations occur, can be estimated *a priori*, it may be advantageous to attempt to use that temperature as a reference point for extrapolation. Indeed, we also found that the error which accumulates in the tunneling region in $\ln \Pi(N)$ is reduced if we use $T^* = 1.20$ as a reference temperature.

B. Binary fluid phase behavior

To demonstrate generalization to multicomponent mixtures, we next consider a simple binary mixture. To the fluid considered in Sec. III A, we add an additional square-well fluid for which $\sigma_{2,2} = \sigma_{1,1} = 1$, $\lambda_{2,2} = \lambda_{1,1} = 1.5$, and $\epsilon_{2,2} = 0.93$. For this second component, the principle of corresponding states suggests a critical temperature of approximately, $k_B T_{c,2}/\epsilon_{1,1} \approx 1.13$, though this is a very rough approximation since the ranges of the interparticle interactions are relatively large and this principle is most accurate when the interactions are more

short-ranged. We employ standard Lorentz-Berthelot mixing rules such that $\epsilon_{1,2} = \sqrt{\epsilon_{1,1}\epsilon_{2,2}}$ and $\sigma_{1,2} = (\sigma_{1,1} + \sigma_{2,2})/2$, and set $\lambda_{1,2} = \lambda_{1,1} = \lambda_{2,2}$. Although this is a relatively simple addition, the size symmetry of this mixture allows us to easily employ both techniques we have discussed to demonstrate the success of our approach. First we consider the results when performing WL-TMMC simulations using the isochoric semigrand ensemble, e.g., we use the total particle number, N_{tot} , as our order parameter for sampling (cf. Appendix B).

Following Ref. 34, we performed a range of simulations at different $\Delta\mu_2$ values for various temperatures. By employing histogram reweighting techniques, we can easily obtain any macrostate distribution at an arbitrary $(\mu_1/\epsilon_{1,1}, \Delta\mu_2^0/\epsilon_{1,1})$ having measured the distribution at $(\mu_1^0/\epsilon_{1,1}, \Delta\mu_2^0/\epsilon_{1,1})$. Fig. 4 shows a comparison between direct simulation and extrapolation from $T^* = 1.35$ down to $T^* = 0.85$, using second order corrections. $T^* = 0.85$ is the lowest temperature we examined and thus represents the most extreme comparison we can make here. We considered a range where $-5.5 \leq \Delta\mu_2/\epsilon_{1,1} \leq 5.5$ which is sufficient to span $0 \leq x_1 \leq 1$ for the computations we report here. Fig. 4(a) shows good agreement again between the extrapolated results and direct simulations at very low temperature, as in the case of the pure component system. In Fig. 4(b) we report the deviation between the two, which again is independent of the choice of $\mu_1/\epsilon_{1,1}$, but does depend on our choice of $\Delta\mu_2/\epsilon_{1,1}$. Regardless, over the range we investigated here we observe a similar maximum in the error in the tunneling region between high and low densities. Although this error is larger than in the pure component case, here we have considered the mixture at $T^* = 0.85$ which is much lower than that considered in Sec. III A ($T^* = 1.05$).

Once again, we seek to compute the phase diagram of this mixture at low temperatures using only the supercritical simulation data. Fig. 5(a) illustrates the phase diagram for the lowest T^* we considered, as well as over the same range as considered in the pure component case. The solid lines (direct simulation)

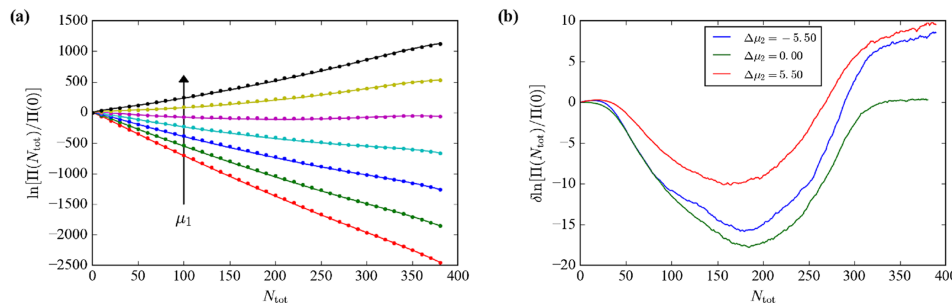


FIG. 4. (a) Comparison between direct simulations (points) of the binary square-well fluid at $T^* = 0.85$ and extrapolation (second order) from $T^* = 1.35$ (lines) at various $-10 \leq \mu_1/\epsilon_{1,1} \leq -2$ when $\Delta\mu_2/\epsilon_{1,1} = 0$. (b) Representative difference at $T^* = 0.85$ between the extrapolated (second order from $T^* = 1.35$) results and those obtained via direct simulation for various $\Delta\mu_2/\epsilon_{1,1}$ values such that $\delta \ln [\Pi(N_{\text{tot}})/\Pi(0)] \equiv \ln [\Pi(N_{\text{tot}})/\Pi(0)]_{\text{ext}} - \ln [\Pi(N_{\text{tot}})/\Pi(0)]_{\text{sim}}$.

agree very well with the predictions made using data obtained at $T^* = 1.35$ (circles). Given the breadth of the diagram, we more carefully consider each individual comparison as well. A representative result for $T^* = 0.85$ is shown in Fig. 5(b). Over intermediate x_1 values, the extrapolated predictions and direct simulation agree very well. The largest deviations in the predicted phase diagrams are observed as the pure-component limits are approached (i.e., $x_1 \rightarrow 1$ or $x_1 \rightarrow 0$). Nonetheless, for intermediate values of x_1 , the predicted vapor pressure of each component is in excellent agreement with those values obtained from direct simulation. The corresponding total density, $\rho_{\text{tot}}\sigma_{1,1}^3 = (N_1 + N_2)\sigma_{1,1}^3/V$, at saturation is shown in Fig. 5(c). Deviations are again only marginal, even at remarkably low temperatures far away from the reference $T^* = 1.35$. As in the pure component instance, this is again a result of the fact that deviations arise primarily in $\ln \Pi(N_{\text{tot}})$ in the transition state region between the two coexisting phases, as depicted in Fig. 5(d) over the range $\Delta\mu_2/\epsilon_{1,1}$ considered here.

Next we studied the same fluid mixture using individual particle numbers as the order parameter for generating the macrostate distribution. This has been explained in detail in

Ref. 53. In this approach, we do not need to extrapolate extensive properties as a function of the order parameter. While this is advantageous for mixtures which are relatively size-symmetric, for highly asymmetric mixtures it can be difficult to define the bounds on, for instance, N_1 given a fixed N_2 . Thus, the previously illustrated approach is potentially more general, at the expense of having to sample more correlations between different extensive variables at each N_{tot} .

Results identical to those in Fig. 5 were obtained, so we simply report the error as a function of the order parameter, \vec{N} , in Fig. 6. At each point in \vec{N} -space we report the error in the canonical partition function, normalized by that obtained from direct simulation. Here, simulations performed at $T^* = 1.35$ were extrapolated using a second order expansion down to $T^* = 0.85$, as in Fig. 5(d). There is an approximate symmetry along the $N_1 = N_2$ curve; if one follows this line, the error profile is similar to that found for $\vec{\Psi} = N_{\text{tot}}$. The overall error is small at low N_{tot} , which goes through a maximum around $N_{\text{tot}} \approx 150$, and then diminishes at higher N_{tot} . Once again, the error principally accumulates in the tunneling region, which does not significantly contribute to the behavior of each phase.

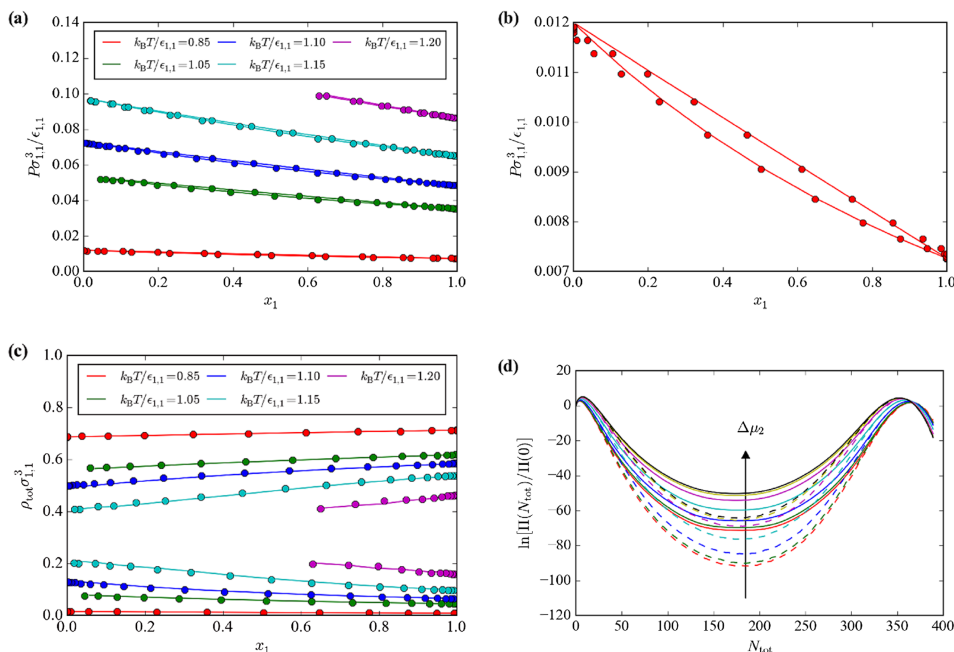


FIG. 5. (a) Coexistence pressure, $P\sigma_{1,1}^3/\epsilon_{1,1}$, versus mole fraction of species 1, x_1 , for the binary square-well fluid from direct simulation (lines) and as predicted by extrapolation from $T^* = 1.35$ (circles). (b) Amplified view of the comparison in (a) for $T^* = 0.85$. (c) Total saturation densities, $\rho_{\text{tot}}\sigma_{1,1}^3$, along the binodal curves from direct simulation and extrapolation in (a). (d) Macrostate distribution at $T^* = 0.85$ from direct simulations (solid lines) and from extrapolating $T^* = 1.35$ data (dashed lines) for a range of $\Delta\mu_2/\epsilon_{1,1}$ values used to construct the phase diagram at this temperature. Colors correspond to specific values of $\Delta\mu_2/\epsilon_{1,1}$.

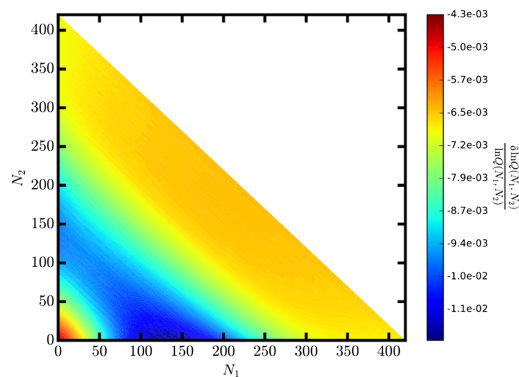


FIG. 6. Relative error in the canonical partition function for the binary square-well fluid, defined as the difference between the surface extrapolated from $T^* = 1.35$ to 0.85 , and that obtained from direct simulation at $T^* = 0.85$, normalized by its value from direct simulation at lower temperature.

C. Confined fluids and wetting behavior

Next we demonstrate the utility of such an extrapolation scheme in predicting the phase behavior of confined fluids. When confined to sufficiently small dimensions, a fluid adsorbed in a pore may undergo capillary condensation. We confined species 1 to a slit-pore, defined by parallel walls separated by $L_z = 8 \sigma_{1,1}$. The box was periodic in the other dimensions, $L_x = L_y = 8 \sigma_{1,1}$. The fluid and the walls were given a square-well interaction, where $\lambda_{1,w} = 1.5$, $\epsilon_{1,w} = 1$ such that

$$U_{1,w}(r') = \begin{cases} \infty, & r' < \sigma_{1,1}/2, \\ -\epsilon_{1,w}, & \sigma_{1,1}/2 \leq r' < \sigma_{1,1}\lambda_{1,w}, \\ 0, & r' \geq \sigma_{1,1}\lambda_{1,w}, \end{cases} \quad (35)$$

where r' is the distance between a particle's center of mass and the face of a wall. Capillary condensation for simple fluids occurs at the point where the $\ln \Pi(N)$ curve develops an asymmetric doubly peaked shape. The low density peak corresponds to fluid adsorbed in layers in the pore, which exhibits a density discontinuity at the Gibbs-dividing surface in the space away from the walls.⁵⁴ The second, broad peak at higher density arises from the state where the pore is filled with condensed fluid. The asymmetric shape of the peaks in $\ln \Pi(N)$ is not a trivial feature, and it is not immediately clear how the error which develops from extrapolating high temperature data will affect this prediction.

In general, however, we find that the approach remains helpful in predicting the macrostate distribution over similar changes in temperature as the bulk. Fig. 7 illustrates the result-

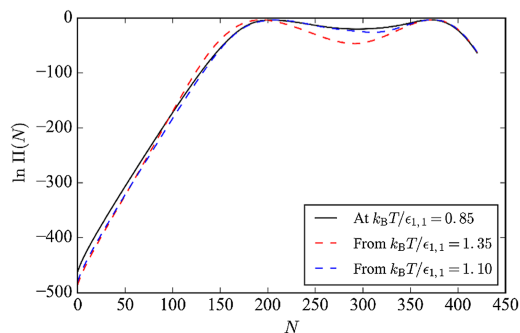


FIG. 7. Macrostate distribution for a pure component square-well fluid of species 1 when confined in a slit-pore. The black curve was obtained by direct simulation at $T^* = 0.85$, which is compared to that estimated from simulations performed at $T^* = 1.35$, and 1.10 via second order extrapolation.

ting $\ln \Pi(N)$ at $T^* = 0.85$ obtained via extrapolation from $T^* = 1.35$ and $T^* = 1.10$ using a second order expansion. Capillary condensation, like bulk condensation, has already occurred at $T^* = 0.85$. The data from $T^* = 1.35$ slightly underpredict the density of the uncondensed phase, while the condensed phase peak is essentially identical to that obtained from direct simulation at this lower temperature. As in the bulk fluid, error principally accumulates in the tunneling region between the phases where correlations are expected to be very high. Extrapolating data which was obtained at $T^* = 1.10$ improves this estimate; higher order extrapolation does as well, however, a second order expansion is sufficient to provide a reasonably accurate estimate of the confined fluid's thermodynamic properties. At the very least, this extrapolated macrostate distribution is quite close to its true value and would require minimal computational effort to refine with an additional relatively short TMMC simulation.

Similarly, this asymmetric $\ln \Pi(N)$ distribution appears during a prewetting transition on flat surfaces, wherein thin and thick liquid films are at coexistence.⁵⁶ An example of this is given in Fig. 8 for a model of argon condensing on solidified carbon dioxide. This has been reproduced from Ref. 55. Here we contrast the quality of different orders of extrapolation. For second order we are able to easily predict data for $T^* = 0.80$ from that obtained at $T^* = 0.90$ with reasonable accuracy; at $T^* \leq 0.75$ further refinement would be necessary. As is often characteristic of third and higher order extrapolation, the predicted surface tends to become noisy although its mean is more closely centered around the true result. This seems to hold true even when extrapolating as low as $T^* = 0.70$. Reduction of the noise in $\ln \Pi(N)$ may be achieved by running longer

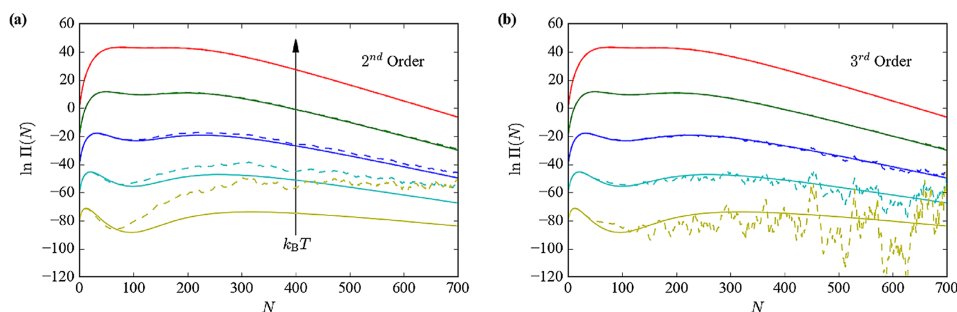


FIG. 8. Comparison between direct simulations (solid lines) and extrapolation from $T^* = 0.90$ down to $T^* = 0.70$ in increments of 0.05 for a model of argon on solidified carbon dioxide described in Ref. 55. Results are reported at the prewetting transition. (a) Extrapolation using up to second order corrections. (b) Extrapolation using up to third order corrections.

simulations at the reference temperature to improve $W(N; \xi^*)$. Higher order estimates strongly depend on the length of the simulation and nature of the system investigated. However, given that a similar issue also occurs for each of the systems we have investigated, using a “noisy” $\ln \Pi(N)$ as an initial guess for further simulations at the target temperature would result in a more efficient use of computational resources.

D. Self-assembly

Until this point, all systems we have considered undergo a first order phase transition upon cooling. Here we assess the capacity of this extrapolation approach to study continuous higher order transitions, such as self-assembly. As a representative system, we consider a recently proposed model for evaluating directional electrostatic interactions in “patchy” particles like proteins and nanocolloids.⁵⁷ Specific details of the model are provided in Ref. 57, and briefly summarized here. In this model, molecules are represented as spherical particles of diameter σ that interact through a steric repulsion and a patchy electrostatic potential, where the latter is represented by the product between a modified isotropic Lennard-Jones (LJ) potential and an angular modulator providing the anisotropy of the potential. Two patches from different particles are considered to interact with each other if both patches are aligned (cf. Fig. 9(a)); the potential yields an attractive (negative) energy if the interacting patches have charges of opposite sign, and a repulsive (positive) energy for patches with like charges (cf. Fig. 9(b)). The angular modulator characterizes both the size and charge distribution of a patch, and it is related to the cosine of the relative orientation between patches with an additional parameter defining the size of the patch (cf. Fig. 9(c)). This model has been shown to capture the rich phase behavior of molecules with specific long-range attractions and repulsions, where the imbalance of these forces determines the order and structural features of the phase separation.⁵⁷ However, in the interest of the current discussion, we restrict the implementation of the extrapolation approach to a system of zwitterionic particles (i.e., particles with one positively and

one negatively charged patch), where the size of each patch is defined by a half opening angle $\delta = 60^\circ$ and a separation between patches of $d = 0.8 \sigma$ (both δ and d are defined in Ref. 57).

In the particular system illustrated here, fluid phase separation is frustrated by the self-assembly of particles; specifically, the formation of entangled chains (cf. Fig. 10(a)). These supramolecular structures are the result of a reduced patch size (akin to other patchy systems⁵⁸) and direct competition between attractive and repulsive forces over a reduced number of orientations. Notably, for systems with equivalent patch sizes but larger separation between patches ($d > 0.8 \sigma$), first order phase separation is dominant over self-assembly.⁵⁷ In terms of the macrostate distribution, self-assembly of this system is characterized by the development of a secondary peak in $\ln \Pi(N)$ at low densities (e.g., for $N=48$ in a simulation box of $V=729 \sigma^3$; see Fig. 10(b)), while the first peak indicates the stable dilute or “gas” phase. The position of the second peak corresponds to the density at which percolation of a single entangled chain is reached. That is, as the number of particles increases, the system transitions from a dilute, monomeric phase to a percolated, single chain. By further increasing N , additional chains are formed (one chain at a time), yielding oscillations in $\ln \Pi(N)$ with a periodicity of $N = 48$. This is a similar behavior to that observed in the self-assembly of other anisotropic particles.^{59,60}

It is therefore critical to correctly predict any subtle changes in curvature of $\ln \Pi(N)$, i.e., the presence of local minima, which delineate the different states of the system which appear as self-assembly begins at low temperature. Fig. 10 depicts both second and third order extrapolation of simulation results from $T^* = 0.125$, where the system exists in a single isotropic fluid phase, to $T^* = 0.12$ ($\Delta\beta^* = 0.33$) which is below the onset temperature of self-assembly. Both capture the low density isotropic vapor phase well, but show some small, systematic deviation in the (first) self-assembled phase. Regardless of that, both predict the weak minimum in $\ln \Pi(N)$ that develops between them. An additional refinement simulation would quickly converge this distribution if further

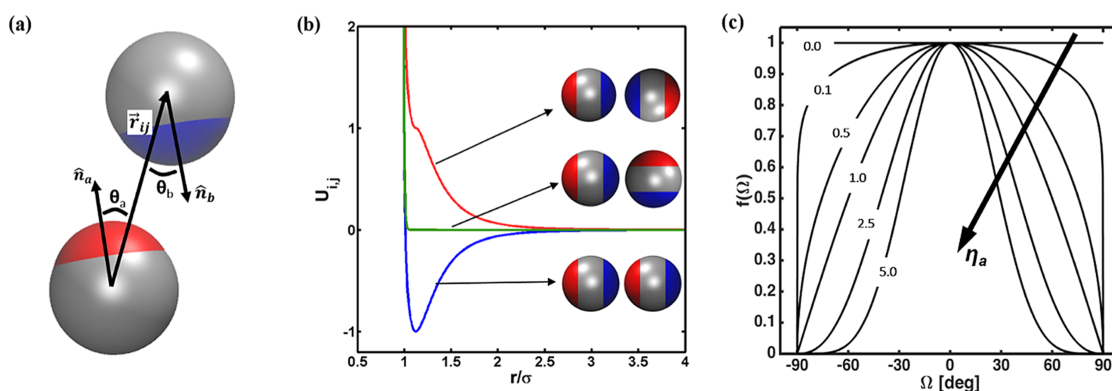


FIG. 9. (a) Schematic representation for the interaction between patchy particles. Each patch is defined by its normal surface vector $\hat{\mathbf{n}}$. Two patches are considered to interact if the characteristic angle of one patch θ_a (given by the opening angle between $\hat{\mathbf{n}}_a$ and the interparticle distance $\vec{\mathbf{r}}_{ij}$) intersects with that of the other patch (i.e., θ_b). (b) Representation of the interaction energy $U_{i,j}$ between two particles for different relative orientations between the patches. (c) Illustrative example of the angular modulator, or the charge distribution, within a single patch ($f(\Omega) = \cos^{\eta_a} \Omega$) for different values of η_a . Ω corresponds to the solid angle between $\hat{\mathbf{n}}_a$ and the reference frame as the particle is rotated.

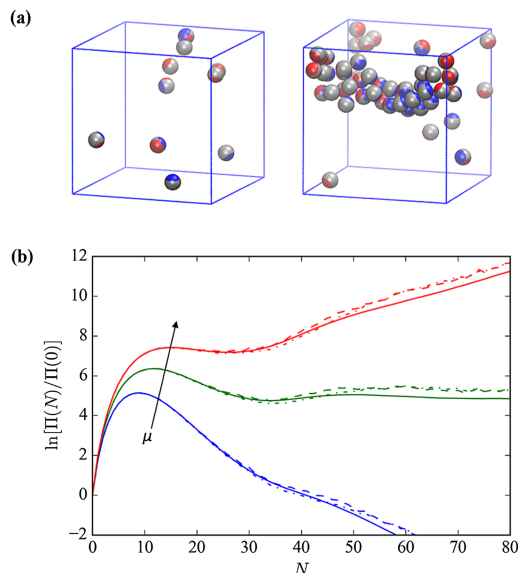


FIG. 10. (a) Illustrative example of the configuration of the monomeric state ($N = 10$, left panel) of patchy particles and the entangled chain ($N = 50$, right panel). (b) Macrostate distribution simulated at $T^* = 0.12$ (solid lines) compared to that obtained from extrapolation of $\ln \Pi(N)$ at $T^* = 0.125$ using second order (dotted-dashed) and third order (dashed) expansions, at various chemical potentials.

quantitative analysis was desired; however, for the purposes of this discussion, it suffices to show that this extrapolation approach is accurate enough to correctly predict the formation of self-assembled aggregates at $T^* = 0.12$.

IV. CONCLUSIONS

Using a Taylor series approach, we have demonstrated a method to extrapolate the free energy landscape and extensive properties obtained from flat-histogram grand canonical Monte Carlo methods between different temperatures. This method follows in the spirit of standard histogram reweighting techniques but does not require histograms to be collected and enumerated at every possible energy and particle number. It also does not require the energy to be discretized and is applicable to scalar order parameters, such as N_{tot} , which simplifies its implementation in biased Monte Carlo simulations. We investigated a range of systems from pure to multicomponent, undergoing first order and continuous phase transitions. Although the accuracy of this approach depends on the system and the quality of the data obtained at the temperature being extrapolated from, we have found that over a range of $-0.25 \lesssim \Delta\beta^* \lesssim 0.25$ second order extrapolation is generally accurate enough to provide a quantitative estimate of thermodynamic properties such as density, pressure, and binodal curves. As such, we have presented simplified expressions for the requisite first and second order derivatives in [Appendices A and B](#) for the interested reader and practitioner.

Furthermore, an estimate of $\ln \Pi(\vec{\Psi})$ at a low temperature, even if it is not sufficiently accurate to perform calculations with, can still be recycled as a starting guess for the biasing function for additional simulations performed at that temperature. Often flat-histogram methods can take a

very long time to converge at low temperatures; a reasonable *a priori* estimate of the macrostate distribution (inverse of the bias) thus has the potential to dramatically reduce the computational cost associated with these simulations by accelerating their convergence. This approach may also be used to provide an estimate of the temperature-activity relationship along the saturation line, which is a key input component to the temperature expanded ensemble method for computing phase coexistence properties recently pursued by the Errington group.⁵¹ An improved initial estimate of the saturation curve is likely to accelerate convergence. In principle, it is also possible to perform similar expansions in other thermodynamic field variables, which is the subject of forthcoming contributions.

ACKNOWLEDGMENTS

Contribution of the National Institute of Standards and Technology, not subject to U.S. Copyright. N.A.M. gratefully acknowledges support from a National Research Council postdoctoral research associateship at the National Institute of Standards and Technology. J.R.E. acknowledges support from the National Science Foundation, Grant No. CHE-1362572.

APPENDIX A: INDIVIDUAL PARTICLE NUMBER SAMPLING

We start from a binary mixture to illustrate our derivations and, by extension, present the results for an arbitrary k -component system at the end. For a binary system in the grand canonical ensemble, the partition function is given by

$$\Xi(\mu_1, \mu_2, V, \beta) = \sum_{N_1} \sum_{N_2} \exp(\beta\mu_1 N_1 + \beta\mu_2 N_2) \times Q(N_1, N_2, V, \beta), \quad (\text{A1})$$

where $Q(N_1, N_2, V, \beta)$ is the canonical partition function for the system, μ_i is the chemical potential of species i , V is the volume, and $\beta = 1/k_B T$. The probability of a given macrostate, defined by the number of particles of each species present, at a given V and β is

$$\ln \Pi(N_1, N_2) = \beta\mu_1 N_1 + \beta\mu_2 N_2 + \ln Q - \ln \Xi. \quad (\text{A2})$$

Our objective is to derive an approximate expression for this macrostate probability distribution at other temperatures (β). In this section we focus on flat-histogram Monte Carlo simulation methods which construct the macrostate probability distribution as a function of the number of particles of each species present, N_1 and N_2 . In [Appendix B](#) we will derive this result when the macrostate probability distribution is sampled according to a different order parameter, $N_{\text{tot}} = \sum_i N_i$, rather than each individual species' particle number.

Following Eq. (20) we must establish expressions for the partial derivatives of $\ln \Pi(N_1, N_2; \beta^0)$. We begin with the first derivative which can be evaluated from Eq. (A2),

$$\frac{\partial \ln \Pi(N_1, N_2)}{\partial \beta} = \mu_1 N_1 + \mu_2 N_2 + \frac{1}{Q} \frac{\partial Q}{\partial \beta} - \frac{1}{\Xi} \frac{\partial \Xi}{\partial \beta}. \quad (\text{A3})$$

The canonical partition function, which has been written implicitly thus far, can be explicitly expressed as

$$Q(N_1, N_2, V, \beta) = \sum_{\nu} O(\nu) \exp(-\beta U(\nu)), \quad (\text{A4})$$

where ν denotes a set of microstates for the system, and O and U are the set's density of states and potential energy, respectively. Thus,

$$\frac{\partial Q}{\partial \beta} = - \sum_{\nu} O(\nu) U(\nu) \exp(-\beta U(\nu)) = -\tilde{U} Q, \quad (\text{A5})$$

where \tilde{U} denotes the canonical ensemble average potential energy. Henceforth in this section, we denote average extensive quantities from the canonical ensemble with a tilde. During a simulation the average potential energy of a given macrostate may be accumulated in a histogram as a function of particle numbers in the same fashion as $\ln \Pi$; thus \tilde{U} is simply an abbreviation for $\tilde{U}(N_1, N_2)$. The derivative of the grand canonical partition function is slightly more involved. After applying the chain-rule this derivative is

$$\begin{aligned} \frac{1}{\Xi} \frac{\partial \Xi}{\partial \beta} &= \frac{1}{\Xi} \sum_{N_1} \sum_{N_2} \left((\mu_1 N_1 + \mu_2 N_2) \exp(\beta \mu_1 N_1 + \beta \mu_2 N_2) Q + \exp(\beta \mu_1 N_1 + \beta \mu_2 N_2) \frac{\partial Q}{\partial \beta} \right) \\ &= \frac{1}{\Xi} \sum_{N_1} \sum_{N_2} \left((\mu_1 N_1 + \mu_2 N_2) \exp(\beta \mu_1 N_1 + \beta \mu_2 N_2) Q - \tilde{U} \exp(\beta \mu_1 N_1 + \beta \mu_2 N_2) Q \right) \\ &= \frac{1}{\Xi} \sum_{N_1} \sum_{N_2} \left((\mu_1 N_1 + \mu_2 N_2 - \tilde{U}) \exp(\beta \mu_1 N_1 + \beta \mu_2 N_2) Q \right) = \langle \mu_1 N_1 + \mu_2 N_2 - \tilde{U} \rangle = \mu_1 \langle N_1 \rangle + \mu_2 \langle N_2 \rangle - \langle U \rangle, \end{aligned} \quad (\text{A6})$$

where the angle brackets denote the average in the grand canonical ensemble. By combining the above equations we arrive at

$$\frac{\partial \ln \Pi(N_1, N_2)}{\partial \beta} = \mu_1 (N_1 - \langle N_1 \rangle) + \mu_2 (N_2 - \langle N_2 \rangle) - (\tilde{U} - \langle U \rangle). \quad (\text{A7})$$

By extension, it is clear that for a k -component system this equation generalizes to

$$\frac{\partial \ln \Pi(N_1, \dots, N_k)}{\partial \beta} = \sum_{i=1}^k \mu_i (N_i - \langle N_i \rangle) - (\tilde{U} - \langle U \rangle). \quad (\text{A8})$$

We now turn our attention to the second derivative. From Eq. (A8) it is clear that this will involve the derivative of grand canonical ensemble averaged extensive properties as well as a single canonical averaged derivative from the potential energy term. The second derivative may be expressed as

$$\frac{\partial^2 \ln \Pi(N_1, \dots, N_k)}{\partial \beta^2} = - \sum_{i=1}^k \mu_i \frac{\partial \langle N_i \rangle}{\partial \beta} - \frac{\partial \tilde{U}}{\partial \beta} + \frac{\partial \langle U \rangle}{\partial \beta}. \quad (\text{A9})$$

The N_i terms in Eq. (A8) are essentially indices of the multi-dimensional histogram of the macrostate probability distribution; this derivative is evaluated at each bin (set of N_i values). Thus, these are constant. The derivatives can be evaluated as follows:

$$\begin{aligned} \frac{\partial \tilde{U}}{\partial \beta} &= \frac{\partial}{\partial \beta} \left(\frac{1}{Q} \sum_{\nu} O(\nu) U(\nu) \exp(-\beta U(\nu)) \right) \\ &= -\tilde{U}^2 + \tilde{U} \tilde{U} \\ &= -\tilde{f}(\tilde{U}, \tilde{U}), \end{aligned} \quad (\text{A10})$$

where the function $\tilde{f}(\tilde{X}, \tilde{Y})$ is used to denote the fluctuation quantity of extensive properties \tilde{X} and \tilde{Y} in the canonical ensemble. In a similar manner,

$$\begin{aligned} \frac{\partial \langle U \rangle}{\partial \beta} &= \frac{\partial}{\partial \beta} \left(\frac{1}{\Xi} \sum_{N_1} \sum_{N_2} \tilde{U} \exp(\beta \mu_1 N_1 + \beta \mu_2 N_2) Q \right) \\ &= \frac{1}{\Xi} \sum_{N_1} \sum_{N_2} \left(\tilde{U} (\mu_1 N_1 + \mu_2 N_2 - \tilde{U}) \exp(\beta \mu_1 N_1 + \beta \mu_2 N_2) Q \right) \\ &\quad - \left(\frac{1}{\Xi} \frac{\partial \Xi}{\partial \beta} \right) \frac{1}{\Xi} \sum_{N_1} \sum_{N_2} \tilde{U} \exp(\beta \mu_1 N_1 + \beta \mu_2 N_2) Q \\ &= \langle \mu_1 N_1 \tilde{U} + \mu_2 N_2 \tilde{U} - \tilde{U}^2 \rangle - \langle U \rangle (\mu_1 \langle N_1 \rangle + \mu_2 \langle N_2 \rangle) - \langle U \rangle \\ &= \mu_1 \hat{f}(\langle U \rangle, \langle N_1 \rangle) + \mu_2 \hat{f}(\langle U \rangle, \langle N_2 \rangle) - \hat{f}(\langle U \rangle, \langle U \rangle), \end{aligned} \quad (\text{A11})$$

where $\hat{f}(\langle X \rangle, \langle Y \rangle) = \langle XY \rangle - \langle X \rangle \langle Y \rangle$ denotes the fluctuation quantity of extensive properties $\langle X \rangle$ and $\langle Y \rangle$ in the grand canonical ensemble. It is clear for a k -component system this may be written as

$$\frac{\partial \langle U \rangle}{\partial \beta} = \sum_{i=1}^k \mu_i \hat{f}(\langle U \rangle, \langle N_i \rangle) - \hat{f}(\langle U \rangle, \langle U \rangle). \quad (\text{A12})$$

In a similar fashion we obtain

$$\frac{\partial \langle N_j \rangle}{\partial \beta} = \sum_{i=1}^k \mu_i \hat{f}(\langle N_j \rangle, \langle N_i \rangle) - \hat{f}(\langle N_j \rangle, \langle U \rangle). \quad (\text{A13})$$

Combining these results we obtain an expression for the second derivative of the macrostate distribution with respect to temperature for a k -component system,

$$\begin{aligned} \frac{\partial^2 \ln \Pi(N_1, \dots, N_k)}{\partial \beta^2} &= 2 \sum_{i=1}^k \mu_i \hat{f}(\langle U \rangle, \langle N_i \rangle) \\ &\quad - \sum_{i=1}^k \sum_{j=1}^k \mu_i \mu_j \hat{f}(\langle N_i \rangle, \langle N_j \rangle) \\ &\quad - \left(\hat{f}(\langle U \rangle, \langle U \rangle) - \tilde{f}(\tilde{U}, \tilde{U}) \right). \end{aligned} \quad (\text{A14})$$

Inserting Eqs. (A8) and (A14) into Eq. (20) we have a second order expansion for the macrostate probability distribution function at any temperature β , given a measured distribution at β^0 . To estimate the properties at a new temperature, we must also extrapolate the histograms of extensive properties measured in the canonical ensemble. In this case, we need only to extrapolate \tilde{U} at each bin according to Eq. (A10) if we employ a first order Taylor series expansion. In this way, at most, only first order correlations between extensive properties must be measured during the simulation. Higher order extrapolation of both the macrostate distribution, as well as extensive properties, may also be done for increased accuracy, though they need not necessarily go up to the same order. Higher order terms of both the macrostate distribution and extensive properties expansions follow directly from subsequent application of chain rules to evaluate further derivatives of Eq. (A14) as discussed in the main text.

APPENDIX B: MULTICOMPONENT SAMPLING IN THE ISOCHORIC SEMIGRAND ENSEMBLE

To simplify the implementation of simulations, it is often convenient to recast the grand canonical partition function in terms of the isochoric semigrand partition function such that we obtain a single order parameter, $N_{\text{tot}} = \sum N_i$, for any multicomponent system. As before, we first consider just a binary mixture,

$$\begin{aligned} \Xi(\mu_1, \Delta\mu_2, V, \beta) &= \sum_{N_{\text{tot}}} \exp(\beta\mu_1 N_{\text{tot}}) \sum_{N_2} \exp(\beta\Delta\mu_2 N_2) Q(N_1, N_2, V, \beta) \\ &= \sum_{N_{\text{tot}}} \exp(\beta\mu_1 N_{\text{tot}}) \Upsilon(N_{\text{tot}}, \Delta\mu_2, V, \beta), \end{aligned} \quad (\text{B1})$$

where $\Delta\mu_2 = \mu_2 - \mu_1$, and for general multicomponent systems $\Delta\mu_i \equiv \mu_i - \mu_1$. $\Upsilon(N_{\text{tot}}, \Delta\mu_2, V, \beta)$ is the isochoric semigrand partition function, which is given by

$$\Upsilon(N_{\text{tot}}, \Delta\mu_2, V, \beta) = \sum_{N_2} \exp(\beta\Delta\mu_2 N_2) Q(N_1, N_2, V, \beta). \quad (\text{B2})$$

For a general k -component system this extends to

$$\begin{aligned} \Upsilon(N_{\text{tot}}, \Delta\mu_2, \dots, \Delta\mu_k, V, \beta) &= \sum_{N_2} \dots \sum_{N_k} \exp(\beta\Delta\mu_2 N_2 + \dots + \beta\Delta\mu_k N_k) \\ &\quad \times Q(N_1, \dots, N_k, V, \beta). \end{aligned} \quad (\text{B3})$$

Therefore, the macrostate probability distribution is given by

$$\ln \Pi(N_{\text{tot}}) = \beta\mu_1 N_{\text{tot}} + \ln \Upsilon - \ln \Xi. \quad (\text{B4})$$

Thus, for a k -component system, all multicomponent effects are contained in Υ . Following Eq. (20) we will seek to find a Taylor Series expansion of the macrostate distribution as temperature changes. To first order, we have

$$\frac{\partial \ln \Pi(N_{\text{tot}})}{\partial \beta} = \mu_1 N_{\text{tot}} + \frac{1}{\Upsilon} \frac{\partial \Upsilon}{\partial \beta} - \frac{1}{\Xi} \frac{\partial \Xi}{\partial \beta}. \quad (\text{B5})$$

As before, we must obtain expressions for this derivative and eventually the second partial derivative of $\ln \Pi$ as well,

$$\frac{1}{\Upsilon} \frac{\partial \Upsilon}{\partial \beta} = \frac{1}{\Upsilon} \sum_{N_2} \left(\Delta\mu_2 N_2 \exp(\beta\Delta\mu_2 N_2) Q + \exp(\beta\Delta\mu_2 N_2) \frac{\partial Q}{\partial \beta} \right) = \frac{1}{\Upsilon} \sum_{N_2} ((\Delta\mu_2 N_2 - U) \exp(\beta\Delta\mu_2 N_2) Q) = \Delta\mu_2 \tilde{N}_2 - \tilde{U} \quad (\text{B6})$$

In this case, the tilde notation indicates an average taken in the isochoric semigrand ensemble, rather than the canonical ensemble as in Appendix A. In other words, \tilde{X} is an extensive quantity that is measured (stored as a histogram) as a function of N_{tot} during simulation. Similar to Eq. (A6),

$$\begin{aligned} \frac{1}{\Xi} \frac{\partial \Xi}{\partial \beta} &= \frac{1}{\Xi} \sum_{N_{\text{tot}}} \sum_{N_2} \left((\mu_1 N_{\text{tot}} + \Delta\mu_2 N_2) \exp(\beta\mu_1 N_{\text{tot}} + \beta\Delta\mu_2 N_2) Q + \exp(\beta\mu_1 N_{\text{tot}} + \beta\Delta\mu_2 N_2) \frac{\partial Q}{\partial \beta} \right) \\ &= \frac{1}{\Xi} \sum_{N_{\text{tot}}} \sum_{N_2} ((\mu_1 N_{\text{tot}} + \Delta\mu_2 N_2) \exp(\beta\mu_1 N_{\text{tot}} + \beta\Delta\mu_2 N_2) Q - U \exp(\beta\mu_1 N_{\text{tot}} + \beta\Delta\mu_2 N_2) Q) \\ &= \frac{1}{\Xi} \sum_{N_{\text{tot}}} \sum_{N_2} ((\mu_1 N_{\text{tot}} + \Delta\mu_2 N_2 - U) \exp(\beta\mu_1 N_{\text{tot}} + \beta\Delta\mu_2 N_2) Q) \\ &= \langle \mu_1 N_{\text{tot}} + \Delta\mu_2 N_2 - U \rangle = \mu_1 \langle N_{\text{tot}} \rangle + \Delta\mu_2 \langle N_2 \rangle - \langle U \rangle. \end{aligned} \quad (\text{B7})$$

By extension, for a general k -component mixture,

$$\frac{\partial \ln \Pi(N_{\text{tot}})}{\partial \beta} = \mu_1 (N_{\text{tot}} - \langle N_{\text{tot}} \rangle) + \sum_{i=1}^k \Delta \mu_i (\tilde{N}_i - \langle N_i \rangle) - (\tilde{U} - \langle U \rangle). \quad (\text{B8})$$

Note that for $i = 1$, $\Delta \mu_1 = 0$, so strictly speaking the first term in the sum does not contribute. We write it only for notational convenience to be formally correct for single component systems as well. Note that the first derivative result is identical to

that obtained in the grand canonical ensemble (cf. Eq. (A8)). Once more, we continue on to the second partial derivative,

$$\frac{\partial^2 \ln \Pi(N_{\text{tot}})}{\partial \beta^2} = -\mu_1 \frac{\partial \langle N_{\text{tot}} \rangle}{\partial \beta} + \sum_{i=1}^k \Delta \mu_i \left(\frac{\partial \tilde{N}_i}{\partial \beta} - \frac{\partial \langle N_i \rangle}{\partial \beta} \right) - \left(\frac{\partial \tilde{U}}{\partial \beta} - \frac{\partial \langle U \rangle}{\partial \beta} \right). \quad (\text{B9})$$

Starting from the derivatives involving isochoric semigrand ensemble averaged extensive quantities, for the potential energy, we have

$$\begin{aligned} \frac{\partial \tilde{U}}{\partial \beta} &= \frac{\partial}{\partial \beta} \left(\frac{1}{\Upsilon} \sum_{N_2} U \exp(\beta \Delta \mu_2 N_2) \mathcal{Q} \right) \\ &= \frac{1}{\Upsilon} \sum_{N_2} U (\Delta \mu_2 N_2 - U) \exp(\beta \Delta \mu_2 N_2) \mathcal{Q} - \left(\frac{1}{\Upsilon} \frac{\partial \Upsilon}{\partial \beta} \right) \left(\frac{1}{\Upsilon} \sum_{N_2} U \exp(\beta \Delta \mu_2 N_2) \mathcal{Q} \right) \\ &= (\Delta \mu_2 \tilde{U} \tilde{N}_2 - \tilde{U}^2) - (\Delta \mu_2 \tilde{N}_2 - \tilde{U}) \tilde{U} = \Delta \mu_2 \tilde{f}(\tilde{U}, \tilde{N}_2) - \tilde{f}(\tilde{U}, \tilde{U}). \end{aligned} \quad (\text{B10})$$

Similarly, it can be shown that

$$\frac{\partial \tilde{N}_1}{\partial \beta} = \Delta \mu_2 \tilde{f}(\tilde{N}_1, \tilde{N}_2) - \tilde{f}(\tilde{U}, \tilde{N}_1). \quad (\text{B11})$$

These expressions generalize for a k -component system such that

$$\frac{\partial \tilde{U}}{\partial \beta} = \sum_{i=1}^k \Delta \mu_i \tilde{f}(\tilde{U}, \tilde{N}_i) - \tilde{f}(\tilde{U}, \tilde{U}) \quad (\text{B12})$$

and

$$\frac{\partial \tilde{N}_j}{\partial \beta} = \sum_{i=1}^k \Delta \mu_i \tilde{f}(\tilde{N}_j, \tilde{N}_i) - \tilde{f}(\tilde{N}_j, \tilde{U}). \quad (\text{B13})$$

The remaining derivatives are with respect to grand canonical ensemble averaged quantities. Consider again the specific case of a binary mixture,

$$\begin{aligned} \frac{\partial \langle N_{\text{tot}} \rangle}{\partial \beta} &= \frac{\partial}{\partial \beta} \left(\frac{1}{\Xi} \sum_{N_{\text{tot}}} N_{\text{tot}} \exp(\beta \mu_1 N_{\text{tot}}) \Upsilon \right) \\ &= \frac{1}{\Xi} \sum_{N_{\text{tot}}} \left(\mu_1 N_{\text{tot}}^2 \exp(\beta \mu_1 N_{\text{tot}}) \Upsilon + N_{\text{tot}} \exp(\beta \mu_1 N_{\text{tot}}) \frac{\partial \Upsilon}{\partial \beta} \right) - \left(\frac{1}{\Xi} \sum_{N_{\text{tot}}} N_{\text{tot}} \exp(\beta \mu_1 N_{\text{tot}}) \Upsilon \right) \left(\frac{1}{\Xi} \frac{\partial \Xi}{\partial \beta} \right) \\ &= \frac{1}{\Xi} \sum_{N_{\text{tot}}} \left((\mu_1 N_{\text{tot}}^2 + N_{\text{tot}} \Delta \mu_2 N_2 - N_{\text{tot}} U) \exp(\beta \mu_1 N_{\text{tot}}) \Upsilon \right) - \left(\frac{1}{\Xi} \sum_{N_{\text{tot}}} N_{\text{tot}} \exp(\beta \mu_1 N_{\text{tot}}) \Upsilon \right) \left(\frac{1}{\Xi} \frac{\partial \Xi}{\partial \beta} \right) \\ &= (\mu_1 \langle N_{\text{tot}}^2 \rangle + \Delta \mu_2 \langle N_{\text{tot}} N_2 \rangle - \langle N_{\text{tot}} U \rangle) - \langle N_{\text{tot}} \rangle (\mu_1 \langle N_{\text{tot}} \rangle + \Delta \mu_2 \langle N_2 \rangle - \langle U \rangle) \\ &= \mu_1 \hat{f}(\langle N_{\text{tot}} \rangle, \langle N_{\text{tot}} \rangle) + \Delta \mu_2 \hat{f}(\langle N_2 \rangle, \langle N_{\text{tot}} \rangle) - \hat{f}(\langle U \rangle, \langle N_{\text{tot}} \rangle). \end{aligned} \quad (\text{B14})$$

Similarly, the other derivatives are as follows:

$$\frac{\partial \langle N_2 \rangle}{\partial \beta} = \mu_1 \hat{f}(\langle N_{\text{tot}} \rangle, \langle N_2 \rangle) + \Delta \mu_2 \hat{f}(\langle N_2 \rangle, \langle N_2 \rangle) - \hat{f}(\langle U \rangle, \langle N_2 \rangle), \quad (\text{B15})$$

$$\frac{\partial \langle U \rangle}{\partial \beta} = \mu_1 \hat{f}(\langle N_{\text{tot}} \rangle, \langle U \rangle) + \Delta \mu_2 \hat{f}(\langle N_2 \rangle, \langle U \rangle) - \hat{f}(\langle U \rangle, \langle U \rangle). \quad (\text{B16})$$

For a general k -component system these may be written as

$$\frac{\partial \langle N_{\text{tot}} \rangle}{\partial \beta} = \mu_1 \hat{f}(\langle N_{\text{tot}} \rangle, \langle N_{\text{tot}} \rangle) - \hat{f}(\langle U \rangle, \langle N_{\text{tot}} \rangle) + \sum_{i=1}^k \Delta \mu_i \hat{f}(\langle N_i \rangle, \langle N_{\text{tot}} \rangle), \quad (\text{B17})$$

$$\frac{\partial \langle N_j \rangle}{\partial \beta} = \mu_1 \hat{f}(\langle N_{\text{tot}} \rangle, \langle N_j \rangle) - \hat{f}(\langle U \rangle, \langle N_j \rangle) + \sum_{i=1}^k \Delta \mu_i \hat{f}(\langle N_i \rangle, \langle N_j \rangle), \quad (\text{B18})$$

$$\frac{\partial \langle U \rangle}{\partial \beta} = \mu_1 \hat{f}(\langle N_{\text{tot}} \rangle, \langle U \rangle) - \hat{f}(\langle U \rangle, \langle U \rangle) + \sum_{i=1}^k \Delta \mu_i \hat{f}(\langle N_i \rangle, \langle U \rangle). \quad (\text{B19})$$

Combining the above results leads to the following expression for the second derivative of the macrostate probability distribution with respect to β :

$$\begin{aligned} \frac{\partial^2 \ln \Pi(N_{\text{tot}})}{\partial \beta^2} &= 2\mu_1 \hat{f}(\langle U \rangle, \langle N_{\text{tot}} \rangle) - \mu_1^2 \hat{f}(\langle N_{\text{tot}} \rangle, \langle N_{\text{tot}} \rangle) - 2\mu_1 \sum_{i=1}^k \Delta \mu_i \hat{f}(\langle N_i \rangle, \langle N_{\text{tot}} \rangle) \\ &\quad - \left(\hat{f}(\langle U \rangle, \langle U \rangle) - \tilde{f}(\tilde{U}, \tilde{U}) \right) - \sum_{i=1}^k \sum_{j=1}^k \Delta \mu_i \Delta \mu_j \left(\hat{f}(\langle N_i \rangle, \langle N_j \rangle) - \tilde{f}(\tilde{N}_i, \tilde{N}_j) \right) \\ &\quad + 2 \sum_{i=1}^k \Delta \mu_i \left(\hat{f}(\langle U \rangle, \langle N_i \rangle) - \tilde{f}(\tilde{U}, \tilde{N}_i) \right). \end{aligned} \quad (\text{B20})$$

Unlike in [Appendix A](#) where only \tilde{U} needed to be extrapolated upon changing β , the other extensive quantities now require this as well. This is because previously the extensive particle numbers defined the order parameters used for sampling, yet here we have reduced this solely to N_{tot} . However, this is simple using a first order Taylor series expansion with Eqs. (B12) and (B13).

- ¹J. W. Tester and M. Modell, *Thermodynamics and its Applications*, 3rd ed. (Prentice Hall, 1997).
- ²D. P. Landau and K. Binder, *A Guide to Monte Carlo Simulations in Statistical Physics* (Cambridge University Press, 2009).
- ³L. P. Kadanoff, "More is the same; phase transitions and mean-field theories," *J. Stat. Phys.* **137**, 777–797 (2009).
- ⁴P. C. Wankat, *Separation Process Engineering* (Pearson Education, 2006).
- ⁵W. J. Koros and R. P. Lively, "Water and beyond: Expanding the spectrum of large-scale energy efficient separation processes," *AIChE J.* **58**, 2624–2633 (2012).
- ⁶C. J. King, *Separation Processes* (Dover Publications, 2013).
- ⁷D. S. Sholl and R. P. Lively, "Seven chemical separations to change the world," *Nature* **532**, 435–437 (2016).
- ⁸P. Horcajada, C. Serre, G. Maurin, N. A. Ramsahye, F. Balas, M. Vallet-Regí, M. Sebban, F. Taulelle, and G. Férey, "Flexible porous metal-organic frameworks for a controlled drug delivery," *J. Am. Chem. Soc.* **130**, 6774–6780 (2008).
- ⁹D. I. Fried, F. J. Brieler, and M. Fröba, "Designing inorganic porous materials for enzyme adsorption and applications in biocatalysis," *ChemCatChem* **5**, 862–884 (2013).
- ¹⁰C. P. Brangwynne, "Phase transitions and size scaling of membrane-less organelles," *J. Cell Biol.* **203**(6), 875–881 (2013).
- ¹¹M. Feric, N. Vaidya, T. S. Harmon, D. M. Mitrea, L. Zhu, T. M. Richardson, R. W. Kriwacki, R. V. Pappu, and C. P. Brangwynne, "Coexisting liquid phases underlie nucleolar subcompartments," *Cell* **165**(7), 1686–1697 (2016).
- ¹²P. Akcora, H. Liu, S. K. Kumar, J. Moll, Y. Li, B. C. Benicewicz, L. S. Schadler, D. Acehan, A. Z. Panagiotopoulos, V. Pryamtsyn, V. Ganesan, J. Ilavsky, P. Thiyagarajan, R. H. Colby, and J. F. Douglas, "Anisotropic self-assembly of spherical polymer-grafted nanoparticles," *Nat. Mater.* **8**(4), 354–359 (2009).
- ¹³J. Russo, P. Tartaglia, and F. Sciortino, "Reversible gels of patchy particles: Role of the valence," *J. Chem. Phys.* **131**(1), 014504 (2009).

- ¹⁴V. Pryamtsyn, V. Ganesan, A. Z. Panagiotopoulos, H. Liu, and S. K. Kumar, "Modeling the anisotropic self-assembly of spherical polymer-grafted nanoparticles," *J. Chem. Phys.* **131**(22), 221102 (2009).
- ¹⁵J. Luiken and P. G. Bolhuis, "Anisotropic aggregation in a simple model of isotropically polymer-coated nanoparticles," *Phys. Rev. E* **88**(1), 012303 (2013).
- ¹⁶A. Nikoubashman, R. A. Register, and A. Z. Panagiotopoulos, "Simulations of shear-induced morphological transitions in block copolymers," *Soft Matter* **9**, 9960–9971 (2013).
- ¹⁷A. Nikoubashman, R. A. Register, and A. Z. Panagiotopoulos, "Self-assembly of cylinder-forming diblock copolymer thin films," *Macromolecules* **46**(16), 6651–6658 (2013).
- ¹⁸A. Nikoubashman, R. L. Davis, B. T. Michal, P. M. Chaikin, R. A. Register, and A. Z. Panagiotopoulos, "Thin films of homopolymers and cylinder-forming diblock copolymers under shear," *ACS Nano* **8**(8), 8015–8026 (2014).
- ¹⁹N. A. Mahynski and A. Z. Panagiotopoulos, "Grafted nanoparticles as soft patchy colloids: Self-assembly versus phase separation," *J. Chem. Phys.* **142**, 074901 (2015).
- ²⁰V. K. Shen, J. K. Cheung, J. R. Errington, and T. M. Truskett, "Coarse-grained strategy for modeling protein stability in concentrated solutions. II: Phase behavior," *Biophys. J.* **90**(6), 1949–1960 (2006).
- ²¹M. A. Floriano, E. Caponetti, and A. Z. Panagiotopoulos, "Micellization in model surfactant systems," *Langmuir* **15**(9), 3143–3151 (1999).
- ²²J. R. Davis and A. Z. Panagiotopoulos, "Monte Carlo simulations of amphiphilic nanoparticle self-assembly," *J. Chem. Phys.* **129**(19), 194706 (2008).
- ²³A. P. Santos and A. Z. Panagiotopoulos, "Determination of the critical micelle concentration in simulations of surfactant systems," *J. Chem. Phys.* **144**(4), 044709 (2016).
- ²⁴T. P. J. Knowles, M. Vendruscolo, and C. M. Dobson, "The amyloid state and its association with protein misfolding diseases," *Nat. Rev. Mol. Cell Biol.* **15**, 384–396 (2014).
- ²⁵N. Metropolis, A. W. Rosenbluth, M. N. Rosenbluth, A. H. Teller, and E. Teller, "Equation of state calculations by fast computing machines," *J. Chem. Phys.* **21**, 1087 (1953).
- ²⁶A. Z. Panagiotopoulos, "Monte Carlo methods for phase equilibria of fluids," *J. Phys.: Condens. Matter* **12**(3), R25–R52 (2000).
- ²⁷D. Frenkel and B. Smit, *Understanding Molecular Simulation: From Algorithms to Applications, of Computational Science Series*, 2nd ed. (Academic Press, 2001), Vol. 1.
- ²⁸A. Z. Panagiotopoulos, N. Quirke, M. Stapleton, and D. J. Tildesley, "Phase equilibria by simulation in the Gibbs ensemble," *Mol. Phys.* **63**(4), 527–545 (1988).

- ²⁹N. B. Wilding and A. D. Bruce, "Density fluctuations and field mixing in the critical fluid," *J. Phys.: Condens. Matter* **4**(12), 3087–3108 (1992).
- ³⁰A. D. Bruce and N. B. Wilding, "Scaling fields and universality of the liquid-gas critical point," *Phys. Rev. Lett.* **68**(2), 193–196 (1992).
- ³¹N. B. Wilding, "Computer simulation of fluid phase transitions," *Am. J. Phys.* **69**(11), 1147–1155 (2001).
- ³²D. P. Landau, S.-H. Tsai, and M. Exler, "A new approach to Monte Carlo simulations in statistical physics: Wang-Landau sampling," *Am. J. Phys.* **72**(10), 1294–1302 (2004).
- ³³J.-S. Wang, T. K. Tay, and R. H. Swendsen, "Transition matrix Monte Carlo reweighting and dynamics," *Phys. Rev. Lett.* **82**(3), 476 (1999).
- ³⁴V. K. Shen and J. R. Errington, "Determination of fluid-phase behavior using transition-matrix Monte Carlo: Binary Lennard-Jones mixtures," *J. Chem. Phys.* **122**(6), 064508 (2005).
- ³⁵J. R. Errington and V. K. Shen, "Direct evaluation of multicomponent phase equilibria using flat-histogram methods," *J. Chem. Phys.* **123**, 164103 (2005).
- ³⁶A. Laio and M. Parrinello, "Escaping free-energy minima," *Proc. Natl. Acad. Sci. U. S. A.* **99**(20), 12562–12566 (2002).
- ³⁷A. Barducci, G. Bussi, and M. Parrinello, "Well-tempered metadynamics: A smoothly converging and tunable free-energy method," *Phys. Rev. Lett.* **100**(2), 020603 (2008).
- ³⁸B. Chen and J. I. Siepmann, "A novel Monte Carlo algorithm for simulating strongly associating fluids: Applications to water, hydrogen fluoride, and acetic acid," *J. Phys. Chem. B* **104**(36), 8725–8734 (2000).
- ³⁹B. Chen and J. I. Siepmann, "Improving the efficiency of the aggregation-volume-bias Monte Carlo algorithm," *J. Phys. Chem. B* **105**(45), 11275–11282 (2001).
- ⁴⁰J. R. Heringa and H. W. J. Blöte, "Geometric cluster Monte Carlo simulation," *Phys. Rev. E* **57**(5), 4976 (1998).
- ⁴¹J. Liu and E. Luijten, "Rejection-free geometric cluster algorithm for complex fluids," *Phys. Rev. Lett.* **92**(3), 035504 (2004).
- ⁴²G. Henkelman, A. Arnaldsson, and H. Jónsson, "A fast and robust algorithm for bader decomposition of charge density," *Comput. Mater. Sci.* **36**(3), 354–360 (2006).
- ⁴³J. J. Potoff and A. Z. Panagiotopoulos, "Critical point and phase behavior of the pure fluid and a Lennard-Jones mixture," *J. Chem. Phys.* **109**, 10914 (1998).
- ⁴⁴D. A. Kofke and E. D. Glandt, "Nearly monodisperse fluids. I. Monte Carlo simulations of Lennard-Jones particles in a semigrand ensemble," *J. Chem. Phys.* **87**, 4881–4890 (1987).
- ⁴⁵D. A. Kofke and E. D. Glandt, "Monte Carlo simulation of multicomponent equilibria in a semigrand canonical ensemble," *Mol. Phys.* **64**, 1105–1131 (1988).
- ⁴⁶M. S. Shell, P. G. Debenedetti, and A. Z. Panagiotopoulos, "An improved Monte Carlo method for direct calculation of the density of states," *J. Chem. Phys.* **119**, 9406 (2003).
- ⁴⁷L. Vega, E. de Miguel, L. F. Rull, G. Jackson, and I. A. McLure, "Phase equilibria and critical behavior of square-well fluids of variable width by Gibbs ensemble Monte Carlo simulation," *J. Chem. Phys.* **96**, 2296 (1992).
- ⁴⁸N. A. Mahynski, L. Rovigatti, C. N. Likos, and A. Z. Panagiotopoulos, "Bottom-up colloidal crystal assembly with a twist," *ACS Nano* **10**, 5459–5467 (2016).
- ⁴⁹K. Binder, "Monte Carlo calculation of the surface tension for two- and three-dimensional lattice-gas models," *Phys. Rev. A* **25**, 1699 (1982).
- ⁵⁰J. K. Singh, D. A. Kofke, and J. R. Errington, "Surface tension of a square-well fluid," *J. Chem. Phys.* **119**(6), 3405–3412 (2003).
- ⁵¹K. S. Rane, V. Kumar, and J. R. Errington, "Monte Carlo methods for computing the wetting and drying properties of model systems," *J. Chem. Phys.* **135**, 234102 (2011).
- ⁵²V. Kumar, S. Sridhar, and J. R. Errington, "Monte Carlo simulation strategies for computing the wetting properties of fluids at geometrically rough surfaces," *J. Chem. Phys.* **135**, 184702 (2011).
- ⁵³J. Mittal, V. K. Shen, J. R. Errington, and T. M. Truskett, "Confinement, entropy, and single-particle dynamics of equilibrium hard-sphere mixtures," *J. Chem. Phys.* **127**, 154513 (2007).
- ⁵⁴D. W. Siderius and V. K. Shen, "Use of the grand canonical transition-matrix Monte Carlo method to model gas adsorption in porous materials," *J. Phys. Chem. C* **117**, 5861–5872 (2013).
- ⁵⁵J. R. Errington, "Prewetting transitions for a model argon on solid carbon dioxide system," *Langmuir* **20**, 3798–3804 (2004).
- ⁵⁶D. Bonn and D. Ross, "Wetting transitions," *Rep. Prog. Phys.* **64**(9), 1085–1163 (2001).
- ⁵⁷M. A. Blanco and V. K. Shen, "Effect of the surface charge distribution on the fluid phase behavior of charged colloids and proteins," *J. Chem. Phys.* **145**, 155102 (2016).
- ⁵⁸E. Bianchi, P. Tartaglia, E. Zaccarelli, and F. Sciortino, "Theoretical and numerical study of the phase diagram of patchy colloids: Ordered and disordered patch arrangements," *J. Chem. Phys.* **128**, 144504 (2008).
- ⁵⁹H. W. Hatch, J. Mittal, and V. K. Shen, "Computational study of trimer self-assembly and fluid phase behavior," *J. Chem. Phys.* **142**(16), 164901 (2015).
- ⁶⁰H. W. Hatch, S.-Y. Yang, J. Mittal, and V. K. Shen, "Self-assembly of trimer colloids: Effect of shape and interaction range," *Soft Matter* **12**(18), 4170–4179 (2016).